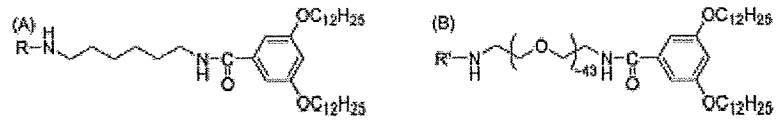

R = Arg4 (Arg4-BDB)
= Arg6 (Arg6-BDB)
= Arg8 (Arg8-BDB)
= Arg10 (Arg10-BDB)

R' = Arg4 (Arg4-PEG-BDB)
= Arg6 (Arg6-PEG-BDB)
= Arg8 (Arg8-PEG-BDB)
= Arg10 (Arg10-PEG-BDB)

Fig. 1. Chemical structures of (Arg)n-BDBs (A) and (Arg)n-PEG-BDBs (B).

with DNA ((Arg)n- or (Arg)n-PEG-L/D, lipoplex) on cellular uptake, gene expression and its mechanism were investigated in human cervical carcinoma HeLa cells. We demonstrate that the different gene expressions between Arg4-L and Arg10-L with or without the PEG spacer may be explained by the different intracellular uptake mechanism by oligoarginine length.

2. Materials and methods

2.1. Materials

Egg phosphatidylcholine (EPC) was purchased from Q.P. Co., Ltd. (Tokyo, Japan). Cholesterol (Chol) and sucrose were from Wako Pure Chemical Industries, Ltd. (Osaka, Japan). The Pica gene luciferase assay kit was purchased from Toyo Ink Mfg. Co., Ltd. (Tokyo, Japan). Bicinchoninic acid (BCA) protein assay reagent was obtained from Pierce (Rockford, IL, USA). DMEM, FBS and FITC-labeled transferrin were purchased from Invitrogen Corp. (Carlsbad, CA, USA). 1,1'-Dioctadecyl-3,3,3',3'-tetramethylindocarbocyanine perchlorate (DiI) was obtained from Lambda Probes & Diagnostics (Graz, Austria). 5-(*N*-Ethyl-*N*-isopropyl)amiloride (EIPA) and filipin were from Sigma Chemical Co. (St. Louis, MO, USA). All other chemicals were of reagent grade. (Arg)n-BDB and (Arg)n-PEG-BDB (Fig. 1A and B) were synthesized as previously reported (Furuhata et al., 2006a,b).

2.2. DNA, rhodamine-labeled DNA and FITC-labeled oligodeoxynucleotide

DNA encoding the luciferase gene under the control of the CMV promoter (pCMV-luc) was constructed as previously described (Igarashi et al., 2006). Protein-free preparation of pCMV-luc was purified following alkaline lysis using maxiprep columns (Qiagen, Hilden, Germany). Labeling of pCMV-luc was performed using the protocol of the Label IT TM-rhodamine labeling kit (Mirus, Madison, WI, USA). The FITC-labeled 20-mer randomized oligodeoxynucleotide (FITC-ODN) was synthesized with a phosphodiester backbone (Sigma Genosys Japan, Hokkaido, Japan).

2.3. Cell culture

HeLa cells were kindly provided by Toyobo Co., Ltd. (Osaka, Japan) and grown in DMEM supplemented with 10% FBS at 37 °C in a humidified 5% CO_2 atmosphere. Cells cultures were prepared by plating cells in a 35-mm culture dish 24 h prior to each experiment.

2.4. Preparation of liposomes

Four liposomal formulae were prepared by the dry film method with water (Furuhata et al., 2006a): EPC, Chol and (Arg)n-BDB or (Arg)n-PEG-BDB in a 7:3:0.5 molar ratio for (Arg)n-L or (Arg)n-PEG-L, respectively. Particle size distributions and zeta-potentials were measured by the dynamic and electrophoresis light scattering method, respectively (ELS-800, Otsuka Electronics Co., Ltd., Osaka, Japan), at 25 °C after the dispersion was diluted to an appropriate volume with water. DiI-labeled liposomes were prepared as described above but with post-addition of DiI at 0.04 mol% of total lipids.

2.5. Gene transfection

Each lipoplex was left at room temperature for 10–15 min. For transfection, (Arg)n-L or (Arg)n-PEG-L/D at a charge ratio (+/−) of (Arg)n-BDB to 2 μg of DNA or FITC-ODN of 1 or 3 was diluted with serum-free DMEM to 1 mL, and then gently applied to the cells. Here, the charge of (Arg)n-BDB or (Arg)n-PEG-BDB was considered the same (+1), not depending on the number of arginine residues.

2.6. Luciferase assay

All samples were incubated with cells for 3 h at 37 °C in serum-free DMEM, DMEM (1 mL) containing 10% FBS was added, and the cells were further incubated for 21 h. Luciferase expression was measured according to the instructions accompanying the Pica gene luciferase assay kit, as described previously (Furuhata et al., 2006b). The protein concentration of the supernatants was determined with BCA reagent using bovine serum albumin (BSA) as the standard, and cps/μg protein was calculated.

2.7. Cellular uptake

(Arg)n-L or (Arg)n-PEG-L/FITC-ODN, (Arg)n-L/FITC-DNA, and DiI-labeled (Arg)n-L/D or (Arg)n-PEG-L/D were diluted with serum-free DMEM to 1 mL, and then gently applied to the cells. In this study, all samples were incubated with cells for 3 h at 37 °C in serum-free DMEM. At the end of the incubation of lipoplexes with cells, the cells were washed three times with 1 mL of PBS, and detached from the plate by incubating with 0.05% trypsin and EDTA solution at 37 °C for 3 min. Flow cytometric analysis was described previously (Furuhata et al., 2006a,b).

To investigate the cellular uptake mechanism, cells were washed with serum-free medium and preincubated for 30 min at 4 °C, or with medium containing sucrose (0.4 M), EIPA (50 μM) or filipin (5 μg/mL) at 37 °C. After the medium was replaced with fresh medium containing complexes, cells were incubated for 1 h at 4 °C, or at 37 °C in the presence of sucrose, EIPA or filipin, and then treated with trypsin before flow cytometry.

2.8. Confocal laser scanning microscopy

To investigate intracellular fate of (Arg)n- and (Arg)n-PEG-lipoplexes in cytoplasm, cells were incubated for 2 and 3 h with DiI-labeled liposomes/FITC-labeled DNA and were observed by confocal microscopy. To investigate cellular uptake mechanism, cells were co-incubated for 1 h with (Arg)n-L or (Arg)n-PEG-L/rhodamine-labeled DNA (+/− = 3/1) with 50 μg/mL FITC-labeled

transferrin. After the medium was removed, the cells were washed five times with PBS. Live cells were observed with a Radiance 2100 confocal laser scanning microscope (BioRad, CA, USA). For DiI-labeled liposome and rhodamine-labeled DNA, maximum excitation was performed by a 543-nm line of internal He-Neon laser, and fluorescence emission was observed with long-pass barrier filter 560DCLP. FITC-labeled DNA and transferrin were imaged using the 488-nm excitation beam of an argon laser, and fluorescence emission was observed with a filter HQ515/30.

2.9. Data analysis

Significant differences in the mean values were evaluated by Student's unpaired *t*-test. A *p*-value of less than 0.05 was considered significant.

3. Results

3.1. Luciferase expression of lipoplexes

We used 5 mol% oligoarginine-modified liposomes because the zeta potential of the prepared liposomes was not increased >5 mol% Arg10 (Furuhata et al., 2006a). Each particle size of liposomes was adjusted to about 200 nm by sonication. Zeta-potentials of (Arg)n-L were increased from 39 to 54 mV as Arg length increased (Furuhata et al., 2006a) while those of (Arg)n-PEG-L did not. The size- and zeta-potentials of lipoplexes at a charge ratio (+/−) of 1/1 and 3/1 were not greatly different (Supplementary Table 1). We evaluated the transfection efficiency of (Arg)n-L or (Arg)n-PEG-L complexed with pCMV-luc ((Arg)n- or (Arg)n-PEG-lipoplexes) at a charge ratio (+/−) of 1/1 in HeLa cells by assaying luciferase activity. The results shown in Fig. 2 demonstrate that longer oligoarginine shows stronger luciferase activity. Decaarginine had the highest

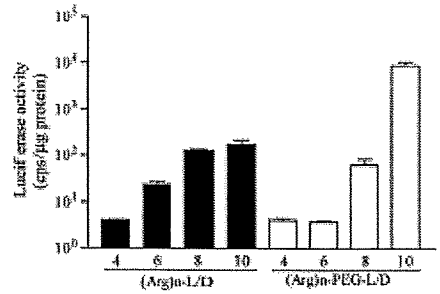

Fig. 2. Luciferase activity after transfection of HeLa cells using (Arg)n- or (Arg)n-PEG-lipoplexes ((Arg)n-L/DB or (Arg)n-PEG-L/DB; 2 μg of DNA = 1:1, (+/−) charge ratio). All samples were incubated with cells for 3 h at 37 °C in serum-free DMEM, and further incubated for 21 h in DMEM containing 10% FBS. Each value is the mean ± S.D. of three separate determinations.

level of activity among the series of liposomes, indicating that the optimal number of arginine residues for transfection was 10 or more. Arg10-PEG-L showed about 50-fold higher transfection efficiency than Arg10-L.

3.2. Cellular uptake of lipoplexes

To confirm the ability of oligoarginine-modified liposomes to carry genes into cells, we assayed the cell internalization of their lipoplexes at a charge ratio (+/−) of 1/1 by flow cytometry (Fig. 3). Cells were exposed for 3 h to the lipoplexes in the absence of serum, and then trypsinized. Flow cytometric analysis confirmed cell internalization. Surprisingly, the cellular uptake of FITC-ODN in (Arg)n- and (Arg)n-PEG-lipoplexes decreased as the number of arginine

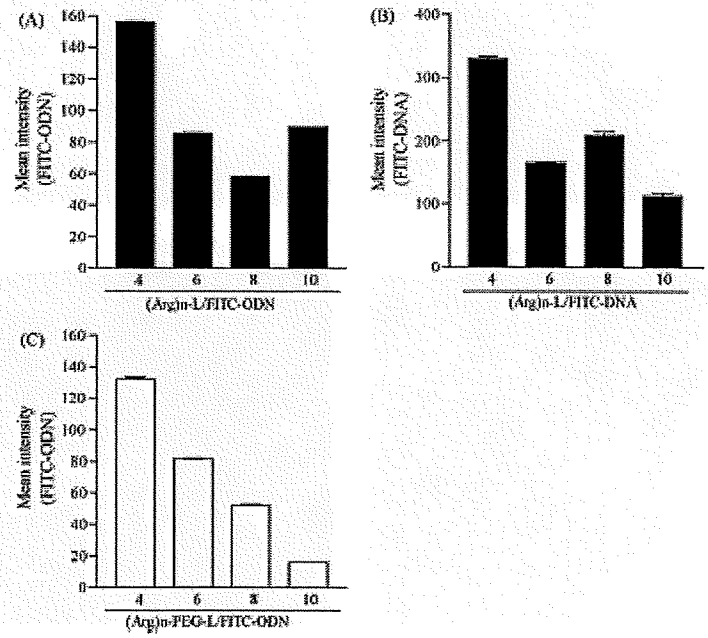

Fig. 3. Cellular uptake of (Arg)n-L/FITC-ODN (A), (Arg)n-L/FITC-DNA (B) and (Arg)n-PEG-L/FITC-ODN (C) lipoplexes at a charge ratio (+/−) of 1/1. Cells were incubated for 3 h in serum-free DMEM and treated with trypsin before FACS analysis. Each bar represents the mean ± S.D. of three experiments.

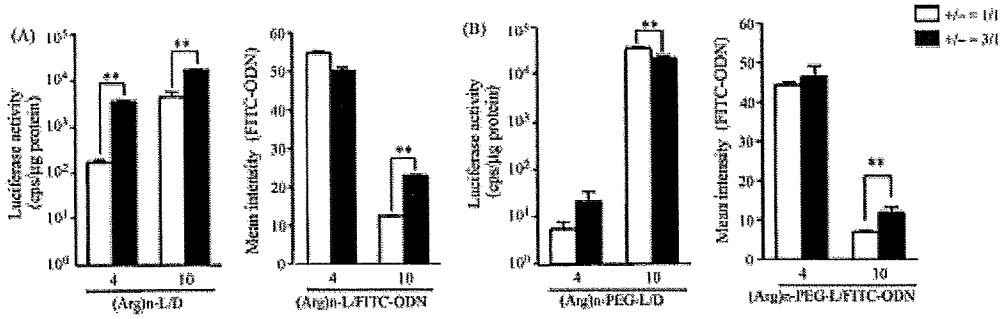

Fig. 4. Influence of charge ratio of Arg4- and Arg10-lipoplexes (A), Arg4-PEG- and Arg10-PEG-lipoplexes (B) on transfection efficiency and cellular uptake (+/− = 1/1 or 3/1). Cellular uptake was examined using FITC-ODN complexes. Each value is the mean ± S.D. of three separate determinations (**$p < 0.01$). The experimental conditions were the same as Fig. 3.

residues increased, except Arg10-L, where Arg4-L and Arg4-PEG-L showed the highest level of FITC-ODN uptake among the series of lipoplexes (Fig. 3A and C). A similar result was obtained when FITC-DNA was used instead of FITC-ODN at a charge ratio (+/−) of 1/1 (Fig. 3B). The difference in transfection efficiency was not correlated with the difference in cellular uptake (Figs. 2 and 3). Hence, we focused on Arg4- or Arg10-modified liposomes in subsequent experiments.

3.3. Effect of the charge ratio (+/−) on luciferase expression and cellular uptake

To examine effect of the charge ratio (+/−) of the delivery of DNA, we increased the charge ratio (+/−) from 1/1 to 3/1 (Fig. 4). When the charge ratio (+/−) was increased at 3/1, the transfection efficiency of Arg4-L and Arg10-L vectors significantly increased, but that of Arg10-PEG-L significantly decreased (Fig. 4A and B) ($p < 0.01$). From

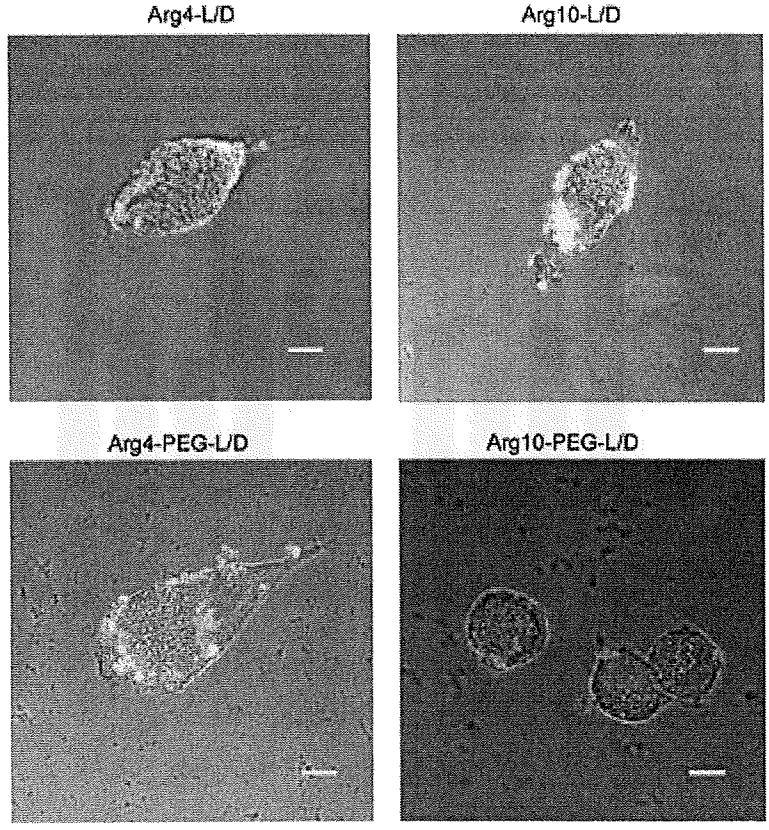

Fig. 5. Release of DNA from (Arg)n- and (Arg)n-PEG-lipoplexes 3 h after transfection by confocal microscopy. DiI-labeled Arg4-, Arg10-, Arg4-PEG- and Arg10-PEG-L (red)/FITC-labeled DNA (green) were incubated for 3 h. Yellow color shows liposomes merged with DNA. Scale bar = 10 μm.

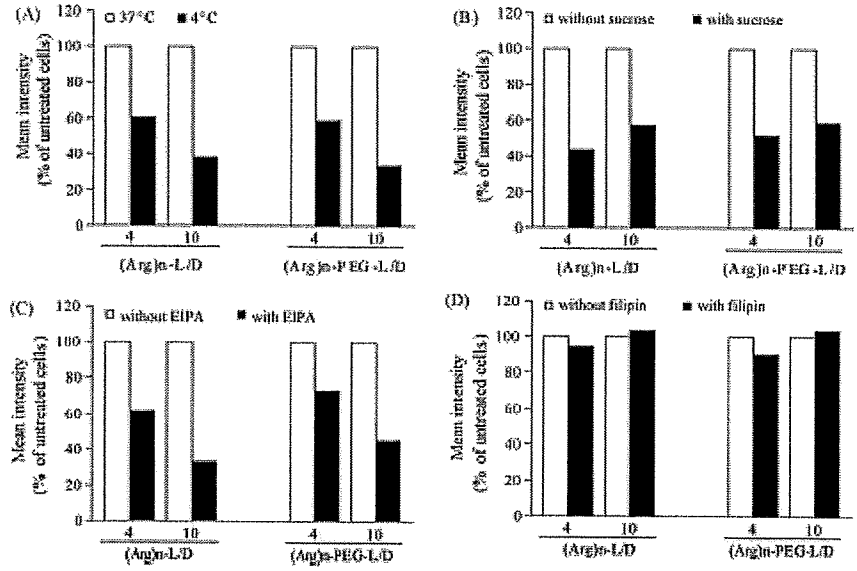

Fig. 6. Mechanism of cellular uptake of (Arg)n- and (Arg)n-PEG-lipoplexes. Effect of low temperature (A), sucrose (B), EIPA (C), and filipin (D) on the cellular uptake of DiI-labeled (Arg)n- and (Arg)n-PEG-lipoplexes at a charge ratio (+/−) = 3/1. HeLa cells were pretreated at 4 °C (A), with sucrose (0.4 M) (B), EIPA (50 μM) (C) or filipin (5 μg/mL) (D) at 37 °C for 30 min. After medium was replaced with fresh medium containing complexes, cells were incubated for 1 h at 4 °C, in the presence of sucrose, EIPA or filipin, and then treated with trypsin before flow cytometry. Each value is the mean of three separate determinations. All values of treated group in (A)–(C) were significantly different from their controls ($p < 0.05$).

the increase of the charge ratio (+/−), cellular uptake of FITC-ODN with Arg10-L and Arg10-PEG-L significantly increased, but that with Arg4-L and Arg4-PEG-L did not (Fig. 4A and B). These findings suggested that Arg4-L and Arg4-PEG-L may be taken up enough, and transfection efficiency may be affected by other factors such as release DNA in the endosome.

3.4. Intracellular fate of lipoplexes in cytoplasm

Because cellular uptake of lipoplexes was not reflected in the transfection efficiency, intracellular fate of (Arg)n- and (Arg)n-PEG-lipoplexes in cytoplasm was examined by colocalization study between DiI-labeled liposomes (red) and FITC-labeled DNA (green) using confocal microscopy. After 2 h-incubation, intracellular (Arg)n- and (Arg)n-PEG-lipoplexes were highly colocalized with DNA (data not shown). After 3 h-incubation, Arg10-PEG-lipoplexes did not show any colocalization whereas other lipoplexes were still colocalized as shown in Fig. 5. This finding suggested that release of DNA from Arg10-PEG-lipoplexes was faster than that from other lipoplexes.

3.5. Mechanism of the cellular uptake of lipoplexes

The difference in the cellular uptake and gene transfection efficiency by oligoarginine-modified liposome may be due to different uptake mechanisms. To investigate the internalization mechanism of (Arg)n- and (Arg)n-PEG-lipoplexes further, we examined the effect of several endocytosis inhibitors on the cellular uptake of DiI-labeled liposomes. Endocytosis is inhibited by low temperature (4 °C) through energy depletion. Cells were exposed to lipoplexes at either 4 °C or 37 °C, then trypsinized, and analyzed by flow cytometry. Low temperature inhibited the uptake of all lipoplexes (Fig. 6A), indicating that transport occurred through energy-dependent endocytosis and supporting the contribution of endocytosis as a major uptake pathway of (Arg)n- and (Arg)n-PEG-lipoplexes. Endocytosis, which occurs in most cells as pinocytosis, represents at least four basic mechanisms: clathrin-mediated endocytosis, macropinocytosis, caveolae-mediated endocytosis, and clathrin- and caveolae-independent endocytosis (Conner and Schmid, 2003). Clathrin-mediated endocytosis is the major endocytotic pathway, and is inhibited by hypertonic medium (0.4 M sucrose), which induces the dissociation of a clathrin lattice (Heuser and Anderson, 1989). In the presence of sucrose, the cellular uptake of Arg4-, Arg10-, Arg4-PEG- and Arg10-PEG-lipoplexes decreased about 57%, 42%, 48% and 41%, respectively, compared with that in the absence of sucrose (Fig. 6B). Macropinocytosis is inhibited by EIPA through the interaction with Na^+/H^+ exchange protein (West et al., 1989). In the presence of EIPA, the cellular uptake of Arg4-, Arg10-, Arg4-PEG- and Arg10-PEG-lipoplexes decreased about 39%, 67%, 27% and 55%, respectively, compared with that in the absence of EIPA (Fig. 6C). Caveolae-mediated endocytosis is inhibited by filipin through cholesterol depletion (Lamaze and Schmid, 1995). Filipin hardly influenced the cellular uptake of all lipoplexes (Fig. 6D), indicating the minor contribution of caveolae in the uptake process. This indicated that Arg10-L and Arg10-PEG-L use macropinocytosis as the major uptake route, whereas Arg4-L and Arg4-PEG-L mainly use a different pathway, probably clathrin-mediated endocytosis.

Furthermore, we examined this by observation of the colocalization of Arg4-, Arg10-, Arg4-PEG- and Arg10-PEG-L/rhodamine-labeled DNA (red) in live cells to intracellular endocytotic vesicles with FITC-labeled transferrin (green), a marker of clathrin-mediated endocytosis (Fig. 7). Arg4- and Arg4-PEG-L/rhodamine-labeled DNA (red) showed colocalization with transferrin, but Arg10- and Arg10-PEG-L/D showed few colocalization with transferrin under the same condition, suggesting that the cellular uptake mechanism was different between Arg4- and Arg4-PEG-L, and Arg10- and Arg10-PEG-L.

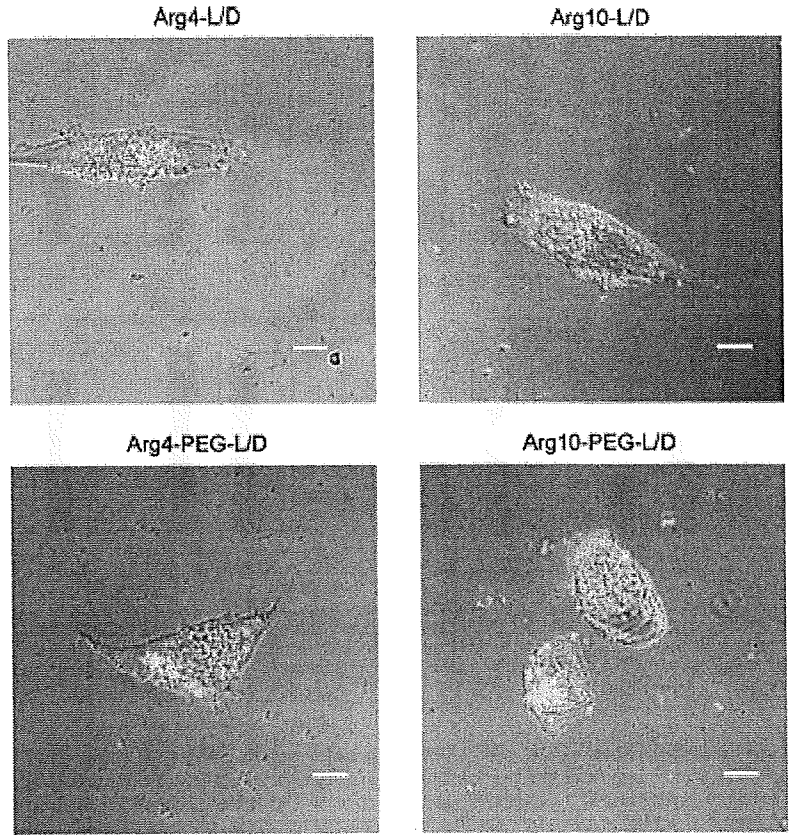

Fig. 7. Cellular uptake mechanism of Arg4-, Arg10-, Arg4-PEG- and Arg10-PEG-lipoplexes. Arg4- Arg10-, Arg4-PEG- and Arg10-PEG-L/rhodamine-labeled DNA (red) and FITC-labeled transferrin (green) were incubated for 1 h and visualized using confocal laser scanning microscopy. Yellow color shows DNA merged with transferrin. Scale bar = 10 μm.

4. Discussion

The cellular uptake of ODN with (Arg)n-L decreased with the increase of oligoarginine length. Moreover, in calcein-entrapped (Arg)n-L as a marker of the aqueous phase, a similar result was obtained by measuring calcein uptake in the cells (Furuhata et al., 2006a). However, the uptake of oligoarginine peptides alone (Wender et al., 2000; Futaki et al., 2001b; Mitchell et al., 2000), and ODN with (Arg)n–PEG–BDB micelle vector (Furuhata et al., 2006b) increased with the increase of oligoarginine length (Supplementary Fig. S1); therefore, this discrepancy may be caused by the uniqueness of liposomes.

Surface functionalization through the PEG spacer would allow oligoarginine flexibility for more efficient interactions with the cell membrane. Torchilin et al. (2001) reported that cellular uptake and the transfection efficiency of Tat peptide attached to the liposome via the PEG spacer were higher than those attached directly to the liposome. In our case, cellular uptake of (Arg)n-PEG-L did not increase depending on oligoarginine length. Furthermore, different from micelle vectors (Furuhata et al., 2006b), the effect of oligoarginine length on the transfection efficiency of oligoarginine-modified liposome was in inverse relation to cellular uptake. Longer arginine length exhibited lower uptake and higher transfection efficiency.

Cellular uptake changes by oligoarginine length in both ODN and DNA in lipoplexes were similar (Fig. 3A and B). To the best of our knowledge, cellular uptake of both DNA and ODN by CPP-modified liposomes has not been reported. We showed that ODN and DNA as lipoplexes were taken up similarly into cells.

Considering that Arg10-L/D and Arg10-PEG-L/D contained more charges than Arg4-L/D and Arg4-PEG-L/D, the increase of charge ratio (+/−) could increase effectively cellular uptake of Arg4-L/D and Arg4-PEG-L/D. In our study, the increase of the charge ratio (+/−) increased cellular uptake of Arg10-L/D and Arg10-PEG-L/D, but not that of Arg4-L/D and Arg4-PEG-L/D. This difference may be explained that Arg4-L and Arg4-PEG-L interacted with DNA stronger than Arg10-L and Arg10-PEG-L, and therefore, could not release DNA. It was supported by the report that Arg4-BDB interacted with DNA stronger than Arg10-BDB (Fujita et al., in press). Another explanation is that the cellular uptake mechanism might be different between them. The increase of the charge ratio (+/−) significantly decreased the transfection efficiency of Arg10-PEG-L vectors despite increased cellular uptake (Fig. 4B). Arg10-PEG-L/D might tightly bind to heparan sulfate proteoglycans (HSP) via PEG spacer. HSP could delay and/or limit the release of lipoplexes in cytosol. These results suggested that intracellular trafficking was one of the rate-limiting stages for transfection efficiency in not only Arg4-L, but also Arg10-L.

The internalization of CPPs was originally described as being unaffected by low-temperature incubation or by treatment with typical endocytosis inhibitors. The pathway was proposed to be

independent of endocytosis (Derossi et al., 1994; Vives et al., 1997); however, later it was reported that this was due to artifacts (Richard et al., 2003). The internalization mechanism of CPP itself or its cargo remains a controversial issue (Nakase et al., 2008). The cellular translocation of Arg4-L and Arg4-PEG-L in lipoplexes decreased by sucrose, but did not decrease much by EIPA compared with Arg10-L and Arg10-PEG-L. Their internalization might involve a different mechanism from macropinocytosis. Furthermore the colocalization image of Arg4- and Arg4-PEG-lipoplexes with transferrin was observed, but that of Arg10- and Arg10-PEG-L was not (Fig. 7). These results suggested that the internalization of Arg10- and Arg10-PEG-lipoplexes (modification with 5 mol% of Arg10) occurs mainly through macropinocytosis, and that of Arg4- and Arg4-PEG-lipoplexes mainly through clathrin-mediated endocytosis. Similar to our result, Khalil et al. (2006) reported that 5 mol% Arg8-modified liposomes containing condensed DNA showed higher gene expression through macropinocytosis.

Decaarginine might induce macropinocytosis because the cellular uptake mechanism of decaarginine-containing vectors, such as Arg10-PEG-BDB micelles (Furuhata et al., 2008), Arg10-L and Arg10-PEG-L, was macropinocytosis, regardless of particle type and the PEG spacer, which exhibited the highest transfection efficiency in a series of oligoarginine vectors. The data suggest the superiority of macropinocytosis as a cellular uptake pathway in gene transfection. It is reported that macropinosomes leak (Meier et al., 2002) and DNA may be released easily into the cytoplasm. Macropinosomes decrease their pH, but do not merge with lysosomes, thus avoiding DNA degradation (Conner and Schmid, 2003).

PEG spacer was more effective for intracellular trafficking than Arg length and surface charge of lipoplex which depends on Arg length at the almost same size of lipoplex. PEG might promote the escape from macropinosomes of DNA because the transfection efficiency of Arg10-PEG-L was significantly higher than that of Arg10-L (Fig. 2) and faster release of DNA from Arg10-PEG-lipoplexes in cytoplasm was observed than Arg10-lipoplexes by confocal microscopy images (Fig. 5).

Liposomes are versatile vectors because they can easily modify their functions by changing components such as oligoarginine lipid and the PEG spacer, maintaining their shape as liposomes.

Acknowledgements

This project was supported in part by a Grant-in-Aid for Scientific Research from the Ministry of Education, Culture, Sports, Science, and Technology of Japan, and by the Open Research Center Project.

Appendix A. Supplementary data

Supplementary data associated with this article can be found, in the online version, at doi:10.1016/j.ijpharm.2008.12.011.

References

Conner, S.D., Schmid, S.L., 2003. Regulated portals of entry into the cell. Nature 422, 37–44.

Derossi, D., Joliot, A.H., Chassaing, G., Prochiantz, A., 1994. The third helix of the *Antennapedia homeodomain* translocates through biological membranes. J. Biol. Chem. 269, 10444–10450.

Fujita, T., Furuhata, M., Hattori, Y., Kawakami, H., Toma, K., Maitani, Y., in press. Calcium enhanced delivery of tetrarginine-PEG-lipid-coated DNA/protamine complexes, Int. J. Pharm, doi:10.1016/j.ijpharm.2008.09.060.

Furuhata, M., Danev, R., Nagayama, K., Yamada, Y., Kawakami, H., Toma, K., Hattori, Y., Maitani, Y., 2008. Decaarginine-PEG-artificial lipid/DNA complex for gene delivery: nanostructure and transfection efficiency. J. Nanosci. Nanotechnol. 8, 2308–2315.

Furuhata, M., Kawakami, H., Toma, K., Hattori, Y., Maitani, Y., 2006a. Intracellular delivery of proteins in complexes with oligoarginine-modified liposomes and the effect of olignarginine length. Bioconjug. Chem. 17, 935–942.

Furuhata, M., Kawakami, H., Toma, K., Hattori, Y., Maitani, Y., 2006b. Design, synthesis and gene delivery efficiency of novel oligo-arginine-linked PEG-lipids: effect of oligo-arginine length. Int. J. Pharm. 316, 109–116.

Futaki, S., Ohashi, W., Suzuki, T., Niwa, M., Tanaka, S., Ueda, K., Harashima, H., Sugiura, Y., 2001a. Stearylated arginine-rich peptides: a new class of transfection systems. Bioconjug. Chem. 12, 1005–1011.

Futaki, S., Suzuki, T., Ohashi, W., Yagami, T., Tanaka, S., Ueda, K., Sugiura, Y., 2001b. Arginine-rich peptides. An abundant source of membrane-permeable peptides having potential as carriers for intracellular protein delivery. J. Biol. Chem. 276, 5836–5840.

Gabizon, A., Horowitz, A.T., Goren, D., Tzemach, D., Mandelbaum-Shavit, F., Qazen, M.M., Zalipsky, S., 1999. Targeting folate receptor with folate linked to extremities of poly(ethylene glycol)-grafted liposomes: in vitro studies. Bioconjug. Chem. 10, 289–298.

Heuser, J.E., Anderson, R.G., 1989. Hypertonic media inhibit receptor-mediated endocytosis by blocking clathrin-coated pit formation. J. Cell Biol. 108, 389–400.

Igarashi, S., Hattori, Y., Maitani, Y., 2006. Biosurfactant MEL-A enhances cellular association and gene transfection by cationic liposome. J. Control. Release 112, 362–368.

Khalil, I.A., Kogure, K., Futaki, S., Harashima, H., 2006. High density of octaarginine stimulates macropinocytosis leading to efficient intracellular trafficking for gene expression. J. Biol. Chem. 281, 3544–3551.

Kogure, K., Moriguchi, R., Sasaki, K., Ueno, M., Futaki, S., Harashima, H., 2004. Development of a non-viral multifunctional envelope-type nano device by a novel lipid film hydration method. J. Control. Release 98, 317–323.

Lamaze, C., Schmid, S.L., 1995. The emergence of clathrin-independent pinocytic pathways. Curr. Opin. Cell Biol. 7, 573–580.

Lewin, M., Carlesso, N., Tung, C.H., Tang, X.W., Cory, D., Scadden, D.T., Weissleder, R., 2000. Tat peptide-derivatized magnetic nanoparticles allow in vivo tracking and recovery of progenitor cells. Nat. Biotechnol. 18, 410–414.

Meier, O., Boucke, K., Hammer, S.V., Keller, S., Stidwill, R.P., Hemmi, S., Greber, U.F., 2002. Adenovirus triggers macropinocytosis and endosomal leakage together with its clathrin-mediated uptake. J. Cell Biol. 158, 1119–1131.

Mitchell, D.J., Kim, D.T., Steinman, L., Fathman, C.G., Rothbard, J.B., 2000. Polyarginine enters cells more efficiently than other polycationic homopolymers. J. Pept. Res. 56, 318–325.

Morris, M.C., Depollier, J., Mery, J., Heitz, F., Divita, G., 2001. A peptide carrier for the delivery of biologically active proteins into mammalian cells. Nat. Biotechnol. 19, 1173–1176.

Nakase, I., Takeuchi, T., Tanaka, G., Futaki, S., 2008. Methodological and cellular aspects that govern the internalization mechanisms of arginine-rich cell-penetrating peptides. Adv. Drug Deliv. Rev. 60, 598–607.

Oehlke, J., Scheller, A., Wiesner, B., Krause, E., Beyermann, M., Klauschenz, E., Melzig, M., Bienert, M., 1998. Cellular uptake of an alpha-helical amphipathic model peptide with the potential to deliver polar compounds into the cell interior non-endocytically. Biochim. Biophys. Acta 1414, 127–139.

Pooga, M., Hallbrink, M., Zorko, M., Langel, U., 1998. Cell penetration by transportant. FASEB J. 12, 67–77.

Richard, J.P., Melikov, K., Vives, E., Ramos, C., Verbeure, B., Gait, M.J., Chernomordik, L.V., Lebleu, B., 2003. Cell-penetrating peptides. A reevaluation of the mechanism of cellular uptake. J. Biol. Chem. 278, 585–590.

Torchilin, V.P., Levchenko, T.S., Rammohan, R., Volodina, N., Papahadjopoulos-Sternberg, B., D'Souza, G.G., 2003. Cell transfection in vitro and in vivo with nontoxic TAT peptide-liposome-DNA complexes. Proc. Natl. Acad. Sci. U.S.A. 100, 1972–1977.

Torchilin, V.P., Rammohan, R., Weissig, V., Levchenko, T.S., 2001. TAT peptide on the surface of liposomes affords their efficient intracellular delivery even at low temperature and in the presence of metabolic inhibitors. Proc. Natl. Acad. Sci. U.S.A. 98, 8786–8791.

Vives, E., Brodin, P., Lebleu, B., 1997. A truncated HIV-1 Tat protein basic domain rapidly translocates through the plasma membrane and accumulates in the cell nucleus. J. Biol. Chem. 272, 16010–16017.

Wender, P.A., Mitchell, D.J., Pattabiraman, K., Pelkey, E.T., Steinman, L., Rothbard, J.B., 2000. The design, synthesis, and evaluation of molecules that enable or enhance cellular uptake: peptoid molecular transporters. Proc. Natl. Acad. Sci. U.S.A. 97, 13003–13008.

West, M.A., Bretscher, M.S., Watts, C., 1989. Distinct endocytotic pathways in epidermal growth factor-stimulated human carcinoma A431 cells. J. Cell Biol. 109, 2731–2739.

The Distribution of mRNA Expression and Protein after Hydrodynamic Injection of Transgene in Mice

Yoshiyuki HATTORI,*[a] Kimiko KOGA,[a] Tomohiro IZUMISAWA,[a] Masahiro YAMASAKI,[b] Ryota NARISHIMA,[b] Saki YOSHIDA,[b] Tetsuya FUKUI,[b] and Yoshie MAITANI[a]

[a] *Institute of Medicinal Chemistry, Hoshi University; and* [b] *Department of Health Chemistry, Hoshi University; 2–4–41 Ebara, Shinagawa-ku, Tokyo 142–8501, Japan.*

Received November 4, 2008; accepted December 26, 2008; published online January 21, 2009

The hydrodynamic method by rapid intravenous injection of a large volume of plasmid DNA is known to be an efficient and liver-specific method of *in vivo* gene delivery and achieves high levels of foreign gene expression, particularly in hepatocytes. Low transgene activities have also been observed in other organs such as the spleen and lung; however, the expression profiles of mRNA and protein are still unknown. Therefore, we investigated the localization of luciferase mRNA by *in situ* hybridization and luciferase activity in mice after transfection of pCMV-luc encoding the luciferase gene under the control of cytomegalo virus (CMV) promoter. We found that hydrodynamic injection effectively induced mRNA expression of the transgene only in the liver although transgene activities were observed in other organs. The transgene activity observed in other organs may be due to leakage from hepatocyte gene expression by transient increase in the permeability of the hepatocyte cellular membrane caused by increased pressure by hydrodynamic injection.

Key words hydrodynamic injection; gene delivery; liver-targeting; gene expression; *in situ* hybridization

The hydrodynamic injection method can provide a route for efficient hepatic expression of transgenes in mice just by systemic administration of naked plasmid DNA.[1—5] It requires the rapid injection of large volume solution (8—9% of body weight), which may alter the physiologic conditions of the liver. Hydrodynamic injection delivery mainly results in expression in the liver,[1,6,7] and has been mostly used to test gene therapy approaches for liver genetic and acquired diseases, including treatments for hemophilia, phenylketonuria, Fabry disease, diabetic nephyropathy, myocarditis, organophoshate toxicity, glomerulonephritis, short-chain acryl-CoA dehydrogenase, obesity, encephalopathy and multiple cancer gene therapy approaches.[6] Recently, hydrodynamic delivery of small interfering RNA (siRNA), short hairpin RNA (shRNA), or plasmid constructs encoding an shRNA has been employed to suppress gene expression in the liver.[6,8,9]

The mechanism of the hydrodynamic injection method which leads to increased liver expression is under investigation by a number of laboratories.[10—12] Moreover, although transgene expression by hydrodynamic injection was also detected at low levels in other organs, such as the lung and spleen,[1,7] it is unclear which cells in the organs expressed the transgene. Furthermore, little is known about the distribution of mRNA expression in organs. Therefore, in this study, to clarify gene expression in other organs we investigated the localization of reporter gene mRNA in mice by *in situ* hybridization and compared with reporter gene activities after transfection with the reporter gene by hydrodynamic injection. Here, we found that hydrodynamic injection effectively induced mRNA expression of the transgene only in the liver although transgene activities were observed in other organs.

MATERIALS AND METHODS

Plasmid pCMV-luc encoding the *firefly* luciferase gene under the control of cytomegalo virus (CMV) promoter was constructed as previously reported.[13] pGL3-basic encoding the *firefly* luciferase gene without a promoter was obtained from Promega (Madison, WI, U.S.A.), and used as a control plasmid. pSV40-gal encoding β-galactosidase under the control of SV40 promoter and enhancer was purchased from Promega (pSV-β-galactosidase control vector). pAlb-gal encoding β-galactosidase under the control of human albumin promoter and SV40 enhancer was obtained from InvivoGen (pDRIVE-SV40/hAlb; CA, U.S.A.) and used as a liver-specific expression plasmid. A protein-free preparation of the plasmids was purified after alkaline lysis in the QIAGEN Endofree Plasmid Maxi kit (Qiagen, Hilden, Germany).

Hydrodynamic Injection Female Balb/c mice (aged 6 weeks, CLEA Japan, Inc., Tokyo, Japan) were used in this study. The mice were maintained in accordance with institutional guidelines of the Hoshi University Animal Care and Use Committee. To transfect plasmid DNA into mice, we used a hydrodynamic injection method: Injection into the tail vein in 5 s with 2.5 ml of saline solution containing 10 μg of pCMV-luc, pGL3-basic, pAlb-gal or pSV40-gal.

Luciferase and β-Galactosidase Activity For *in vivo* imaging analysis, 24 h after hydrodynamic injection, D-luciferin (potassium salt) dissolved in phosphate-buffered saline (PBS) (125 mg/kg of body weight) was injected into the mouse peritoneal cavity and subsequently anesthetized by intramuscular injection of 50 mg/kg body weight of pentobarbital (Nembutal, Dainippon Pharmaceutical Co., Ltd., Osaka, Japan). *In vivo* bioluminescence imaging was performed using an NightOWL LB981 NC100 system (Berthold Technologies, Bad Wildbad, Germany). A gray scale body-surface reference image was collected using an NightOWL LB981 CCD camera as previously reported.[14]

For luciferase and β-galactosidase activities from homogenated tissues, 12, 24 or 48 h after plasmid injection, mice were anesthetized and sacrificed. Different organs, including the liver, spleen, lung, heart and kidney, were dissected from dead animals using standard surgical procedures. One milliliter of lysis buffer (25 mM Tris–HCl, 2 mM diaminocyclohexane–diamine tetraacetic acid (CDTA), 2 mM dithiothreitol (DTT), 10% glycerol and 1% Triton X-100,

* To whom correspondence should be addressed. e-mail: yhattori@hoshi.ac.jp

pH 7.8) for luciferase assay and of reporter lysis buffer (Promega) for β-galactosidase assay was added to the whole organ of the kidney, spleen, lung and heart. Each organ was homogenized for 15—20 s at maximal speed and tissue homogenates were then centrifuged in a microcentrifuge for 5 min at 15000 rpm at 4 °C. Luciferase expression was measured as counts per sec (cps)/mg protein using the luciferase assay system (Pica gene; Toyo Ink Mfg. Co., Ltd., Tokyo, Japan) and BCA reagent (Pierce, Rockford, IL, U.S.A.) as previously reported.[14] β-Galactosidase expression was measured as counts per sec (cps)/mg protein using the Beta-Glo assay system (Promega).

Preparation of Probes for *in Situ* Hybridization The cDNA fragment (611 bp) of *firefly* luciferase was amplified from pGL3-basic. The oligonucleotide primers used for amplification were: forward (5′-gaacgtgaattgctcaacag-3′) and reverse (5′-gaagcaatttcgtgtaaattag-3′) for luciferase. The fragments were cloned into pGEM-T vector (Promega). ^{35}S-Labeled cRNA probes were transcribed from cloned cDNA as a template with SP6 or T7 RNA polymerase (Takara Bio Inc., Japan) in the presence of 5′-α-[^{35}S]thiotriphosphate (*ca.* 30 TBq/mmol) (GE Healthcare Bio-sciences Co., Buckinghamshire, England). The probes were shortened to an average length of 200 bases by alkaline hydrolysis.

***In Situ* Hybridization** The liver, kidney, heart, spleen, lung and brain from adult female Balb/c mice (6 weeks) 24 h after hydrodynamic injection of pCMV-luc or pGL3-basic were frozen in powdered dry ice, and coronal sections were cut 16 μm thick with a cryostat, thaw-mounted onto gelatin and poly-lysine coated slides, and stored at −80 °C until hybridization. Sections were fixed in 4% formaldehyde/10 mM PBS for 15 min at room temperature, rinsed in PBS for 3 min, and treated with 0.125 μg/ml proteinase K at 37 °C for 10 min. After rinsing in PBS, they were immersed in 0.25% acetic anhydride in 75 mM triethanolamine/0.9% NaCl for 10 min and dehydrated through an ethanol series (70%, 85%, 95%, 100%). Tissue sections were prehybridized at 55 °C for 1 h in hybridization solution (50% formamide, 4×SSC, 2.5×Denhardt's solution, 5 mM ethylenediaminetetraacetic acid (EDTA), pH 8.0, 100 μg/ml heat-denatured salmon sperm DNA, 20 mM DTT), followed by hybridization at 55 °C for 16 h in hybridization solution containing 10% dextran sulfate and a ^{35}S-labeled cRNA probe of the luciferase gene. Thereafter, the sections were rinsed four times at 55 °C for 10 min in 2×SSC/10 mM 2-mercaptoethanol, treated with RNase A (40 μg/ml in 0.5 M NaCl 10 mM Tris–HCl, 1 mM EDTA, pH 8.0) at 37 °C for 30 min, washed twice at 55 °C for 30 min in 50% formamide/2×SSC, and rinsed once at room temperature for 10 min in 2×SSC/10 mM 2-mercaptoethanol. The washed sections were dehydrated with ethanol, air-dried and exposed Hyperfilm ECL (GE Healthcare Bio-sciences Co.) for 10 d. To determine the regional localization of luciferase mRNA, labeled sections were dipped in liquid emulsion (Kodak NTB3; Kodak, Rochester, U.S.A.) diluted 1 : 1 with water, and exposed for 3 weeks. After development, all sections were counterstained with hematoxylin and eosin.

Determination of Plasma Transaminase Activities Serum was prepared by separation of the coagulated whole blood of animals 1 d after injection of 2.5 ml of plasmid DNA solution. Aspartate aminotransferase (AST/GOT) and alanine aminotransferase (ALT/GPT) activities in the plasma were determined by commercially available test reagents (GPT-UV test Wako and GPT-UV test Wako, respectively; Wako, Osaka, Japan). Normal values were determined using blood obtained from age-matched, untreated mice.

Statistical Analysis Significant differences in mean values were evaluated using Student's unpaired *t*-test. A *p*-value of <0.05 was considered significant.

RESULTS AND DISCUSSION

First, to examine which tissue gene expression was induced by hydrodynamic injection, we injected 10 μg of plasmid DNA and measured luciferase activity 12, 24 or 48 h after the hydrodynamic injection into mice (Figs. 1A—C). We measured luciferase activity from homogenized tissues (Figs. 1A, B) and imaged mice using an NightOWL LB981 NC100 system (Fig. 1C). Among the organs in mice transfected with pCMV-luc 12 and 24 h after transfection, extensive luciferase activity was detected in the liver, and low activity was detected in the spleen, kidney, heart and lung (Fig. 1A). Luciferase activity in serum was higher than in the spleen, kidney, heart and lung at 12 and 24 h after transfection although luciferase is a cytosolic protein, not secretable from cells. In mice transfected with pGL3-basic, luciferase activity was not detected in any organs (Figs. 1B, C).

To examine whether high luciferase activity in serum until 24 h after injection was maintained through increased permeability of the cell membrane of hepatocytes with a high level of luciferase activity, hepatic enzymes, ALT and AST, were measured as indicators of liver damage. Figure 1D shows the plasma concentration profiles of ALT and AST following hydrodynamic injection of pCMV-luc or pGL3-basic solution. The levels of ALT and AST in mice transfected by hydrodynamic injection markedly increased from the normal levels of 7 and 22 IU/l to 270 and 360 IU/l in mice transfected with pGL3-basic and to 235 and 353 IU/l in mice with pCMV-luc, respectively. This finding corresponded with the report that the hydrodynamics-based procedure caused transient liver damage with high serum ALT and AST levels, which rapidly returned to normal in a few days,[7] suggested that luciferase activity in serum may be due to the transiently increased permeability of hepatocyte cellular membrane by hydrodynamic injection.

Next, we investigated the localization of luciferase mRNA by *in situ* hybridization 24 h after transfection of pCMV-luc or pGL3-basic by hydrodynamic injection. The sense probe for the luciferase gene was used as a negative control probe. Positive cells for luciferase mRNA were strongly detected in the liver by hybridization with the antisense probe for the luciferase gene (Fig. 2). Silver grain distribution in the dark field following *in situ* hybridization exhibited luciferase mRNA expression (Figs. 3A, B). Less than 10% of liver cells were positive for the expression of luciferase mRNA (Fig. 3A) and positive cells at high grain density were mainly hepatocytes (Fig. 3B); however, luciferase mRNA was not detected in the spleen, kidney, brain, heart and lung (Figs. 2, 3A), although luciferase activity was detected (Fig. 1A).

Transcription of the albumin gene occurs almost exclusively in the liver and is controlled by a strong liver-specific promoter.[15—17] pAlb-gal with liver-specific albumin pro-

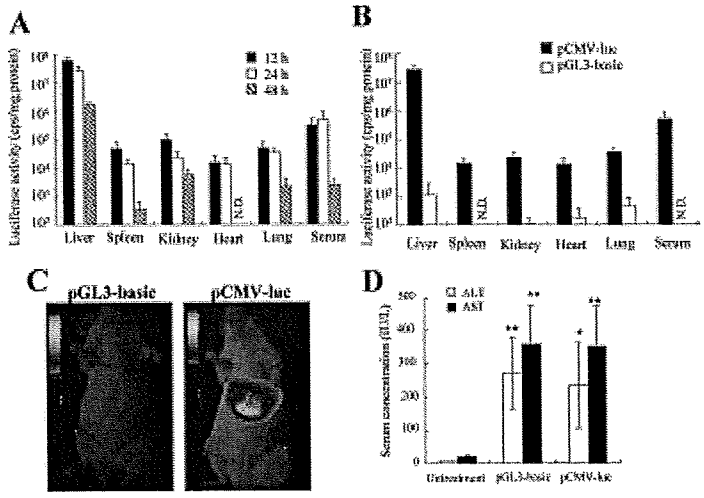

Fig. 1. Luciferase Activity and Toxicity in Mice after Hydrodynamic Injection

(A) Luciferase activity from tissue homogenate 12, 24, 48 h after hydrodynamic injection of pCMV-luc. (B) Luciferase activity from tissue homogenate 24 h after hydrodynamic injection of pCMV-luc and pGL3-basic as a control plasmid. Each bar in A and B represents the mean±S.D. (n=3—5). N.D., not detected. (C) Luciferase activity by bioluminescent imaging 24 h after hydrodynamic injection. (D) Profiles of plasma transaminase activities following hydrodynamic injection into mice. Mice received a large-volume intravenous injection of pCMV-luc or pGL3-basic solution and blood was collected at 24 h. Plasma ALT and AST activities were determined. Control represents age-matched, untreated mice. The results are expressed as the mean±S.D. (n=4).

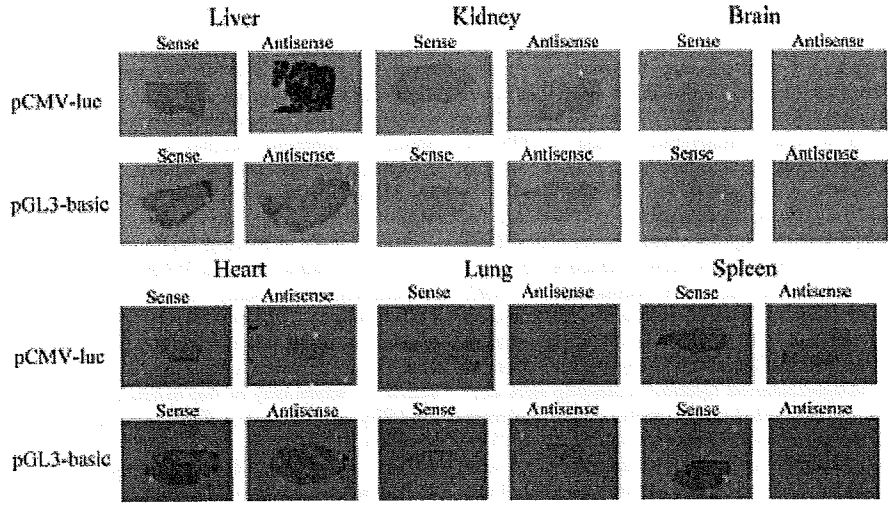

Fig. 2. *In Situ* Hybridization of a ^{35}S-Labeled Antisense or Sense Probe Generated against Luciferase mRNA

Macroautoradiographs shows the expression of luciferase mRNA 24 h after hydrodynamic injection.

moter can induce the expression of β-galactosidase, especially in the liver and pSV40-gal in ubiquitous organs. To investigate whether pAlb-gal induced β-galactosidase activity in only the liver, we transfected pAlb-gal into mice and then compared β-galactosidase activity with that of pSV40-gal. The pattern of β-galactosidase activities in mice transfected with pAlb-gal was similar to that in mice with pSV40-gal (Fig. 4). β-Galactosidase activity was also detected in serum although β-galactosidase protein is a cytosolic protein. These data indicated that the β-galactosidase activities detected in organs other than the liver could be attributed to release from hepatocytes by transient permeability of the cellular membrane. The β-galactosidase and luciferase proteins circulating in blood might cause the activities in the other organs.

The increased volume and pressure of direct injection into liver vessels was initially proposed as a means to increase the size of the sinusoid fenestae, thereby increasing extravasation and delivery of plasmid DNA to liver cells; however, the mechanism of gene transfer is not clearly understood. Although both luciferase and β-galactosidase proteins were not secretable, activities were detected in the serum after transfection by hydrodynamic injection (Figs. 1A, 4). The half-

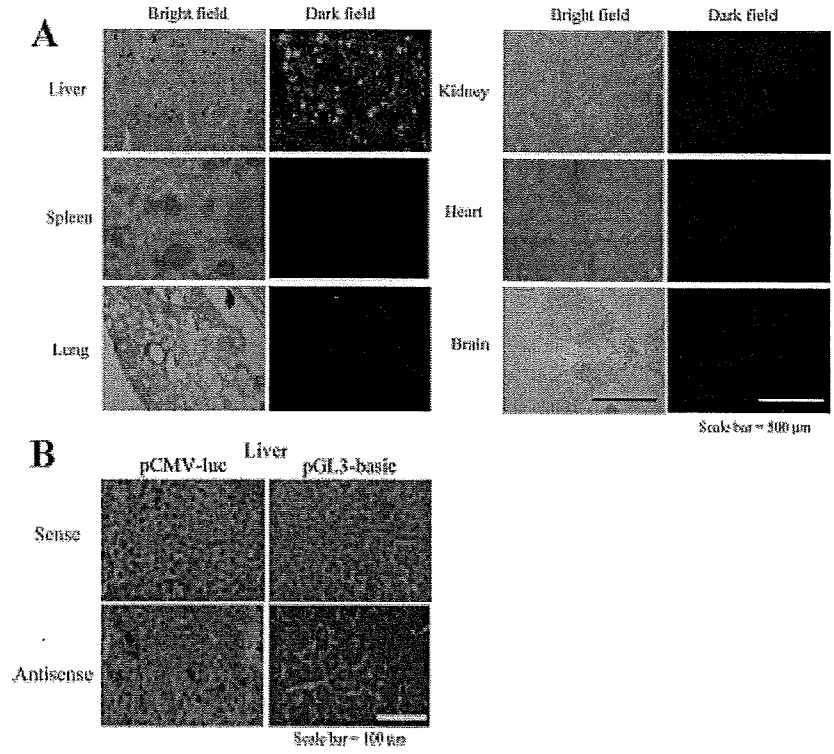

Fig. 3. *In Situ* Hybridization of a ^{35}S-Labeled Antisense or Sense Probe Generated against Luciferase mRNA

In A, antisense probe was used for detection of luciferase mRNA. Microautoradiographs in bright and dark fields show the expression of luciferase mRNA 24 h after hydrodynamic injection. Silver grains in dark field and black grains in bright field indicate luciferase mRNA expression. Scale bar: 500 μm. In B, microautoradiographs show the expression of luciferase mRNA in liver 24 h after hydrodynamic injection. The sense probe for the luciferase gene was used as a negative control probe. Scale bar: 100 μm.

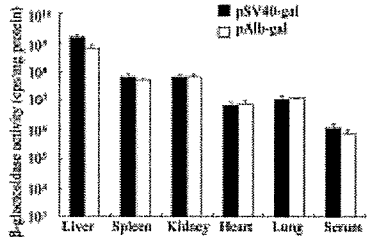

Fig. 4. β-Galactosidase Activity in Mice by Transfection of Plasmid DNA with Liver-Specific Promoter

β-Galactosidase activity from tissue homogenate 24 h after hydrodynamic injection of pAlb-gal and pSV40-gal. The results are expressed as the mean ± S.D. (n=3).

life of luciferase protein was about 10 min when incubated with mouse serum at 37 °C (data not shown), indicating that high luciferase activity in serum 12 and 24 h after transfection was supplied from highly sustained hepatocyte gene expression.

Hepatocyte membrane pores after hydrodynamic injection have been observed using scanning electron microscopy.[18] Elevated ALT and AST blood levels after injection are also consistent with the appearance of membrane pores.[19] Leakage of these enzymes is not totally due to cellular apoptosis or necrosis. The necrotic areas were less than 1% of the liver following hydrodynamic injection.[17] When propidium iodide (PI), which is not supposed to cross the plasma membrane of viable cells, was effectively incorporated into liver cells (10% of hepatocytes) by hydrodynamic injection, PI-positive cells were not likely to be dead cells, and the time-dependent elimination of PI intensity was observed from viable cells.[7] These findings suggested that the apparent increased permeability of the cell membrane may be caused by the invasive nature of the hydrodynamic injection.

From our results, hydrodynamic injection could effectively induce the expression of transgene mRNA in the liver, but not in other organs or under the detection limit of analysis by *in situ* hybridization. The hydrodynamic injection method induced gene expression in the liver, which leaked transgene protein from hepatocytes through the transiently increased permeability of the cellular membrane, eventually carrying it in the bloodstream to other organs. Interpretation of the gene expression in other organs by hydrodynamic injection will be needed to require caution. This information is of value to predict the distribution of therapeutic transgene proteins induced by the hydrodynamic injection method.

Acknowledgments This project was supported in part by Grants-in-Aid for Scientific Research from the Ministry of Education, Culture, Sports, Science and Technology of Japan, and by the Open Research Center Project.

REFERENCES

1) Liu F., Song Y., Liu D., *Gene Ther.*, **6**, 1258—1266 (1999).
2) Al-Dosari M. S., Knapp J. E., Liu D., *Adv. Genet.*, **54**, 65—82 (2005).
3) Hodges B. L., Scheule R. K., *Expert Opin. Biol. Ther.*, **3**, 911—918 (2003).
4) Knapp J. E., Liu D., *Methods Mol. Biol.*, **245**, 245—250 (2004).
5) Suda T., Liu D., *Mol. Ther.*, **15**, 2063—2069 (2007).
6) Herweijer H., Wolff J. A., *Gene Ther.*, **14**, 99—107 (2007).
7) Kobayashi N., Nishikawa M., Hirata K., Takakura Y., *J. Gene Med.*, **6**, 584—592 (2004).
8) Lewis D. L., Hagstrom J. E., Loomis A. G., Wolff J. A., Herweijer H., *Nat. Genet.*, **32**, 107—108 (2002).
9) McCaffrey A. P., Meuse L., Pham T. T., Conklin D. S., Hannon G. J., Kay M. A., *Nature* (London), **418**, 38—39 (2002).
10) Sebestyen M. G., Budker V. G., Budker T., Subbotin V. M., Zhang G., Monahan S. D., Lewis D. L., Wong S. C., Hagstrom J. E., Wolff J. A., *J. Gene Med.*, **8**, 852—873 (2006).
11) Budker V. G., Subbotin V. M., Budker T., Sebestyen M. G., Zhang G., Wolff J. A., *J. Gene Med.*, **8**, 874—888 (2006).
12) Suda T., Gao X., Stolz D. B., Liu D., *Gene Ther.*, **14**, 129—137 (2007).
13) Igarashi S., Hattori Y., Maitani Y., *J. Controlled Release*, **112**, 362—368 (2006).
14) Hattori Y., Ding W. X., Maitani Y., *J. Controlled Release*, **120**, 122—130 (2007).
15) Hsiang C. H., Marten N. W., Straus D. S., *Biochem. J.*, **338**, 241—249 (1999).
16) Power S. C., Cereghini S., Rollier A., Gannon F., *Biochem. Biophys. Res. Commun.*, **203**, 1447—1456 (1994).
17) Herweijer H., Zhang G., Subbotin V. M., Budker V., Williams P., Wolff J. A., *J. Gene Med.*, **3**, 280—291 (2001).
18) Zhang G., Gao X., Song Y. K., Vollmer R., Stolz D. B., Gasiorowski J. Z., Dean D. A., Liu D., *Gene Ther.*, **11**, 675—682 (2004).
19) Rozmanith W., Chabicovsky M., Herkner K., Schulte-Hermann R., *DNA Cell Biol.*, **21**, 847—853 (2002).

European Journal of Medicinal Chemistry 44 (2009) 4603–4610

Contents lists available at ScienceDirect

European Journal of Medicinal Chemistry

journal homepage: http://www.elsevier.com/locate/ejmech

Original article

Histone deacetylase inhibitor prodrugs in nanoparticle vector enhanced gene expression in human cancer cells

Yuta Ishii [a], Yoshiyuki Hattori [b], Toshiharu Yamada [a], Shinichi Uesato [a], Yoshie Maitani [b], Yasuo Nagaoka [a,*]

[a] Faculty of Chemistry, Materials and Bioengineering, Kansai University, Suita, Osaka 564-8680, Japan
[b] Institute of Medicinal Chemistry, Hoshi University, Shinagawa, Tokyo 142-8501, Japan

ARTICLE INFO

Article history:
Received 14 May 2009
Received in revised form
15 June 2009
Accepted 28 June 2009
Available online 4 July 2009

Keywords:
Non-viral vector
Histone deacetylase inhibitor
Cationic nanoparticle
HDAC
Cationic cholesterol
Gene expression

ABSTRACT

We developed histone deacetylase inhibitor (HDACI) prodrugs to enhance the expression of the external genes transfected into human cells with cationic nanoparticles (NPs). We synthesized five kinds of lipid-linked HDACI prodrugs in which *n*-dodecanoic acid or cholesterol is linked with a potent HDACI, K-182, by an ester bond or a disulfide carbonate linker. The prodrugs were able to admix as a component of NPs, although the intact K-182 was not incorporated into NPs. Namely, NPs composed of cholesteryl-3β-carboxyamidoethylene-*N*-hydroxyethylamine and Tween 80 with the 10 mol% K-182 prodrug were prepared as a DNA vector to transfect plasmid DNAs into human prostate cancer cells, PC-3, or human breast cancer cells, Sk-Br-3. The NPs containing K-182 prodrugs with *n*-dodecanoic acid exhibited two to four times higher the gene expression than the original NPs. The enhancement of the gene expression will be due to the hyperacetylation of core histones caused by intact K-182 degraded from the prodrug in the vector incorporated into the cells.

1. Introduction

Development of an efficient and safe method for the delivery of exogenous DNAs into mammalian cells is critical both for basic biosciences and clinical applications, including iPS cell techniques and gene therapy. Viral vectors have been used for this purpose because of their high transfection efficiency, but disadvantages such as pathogenicity, immunogenicity, mutational potential and low capacity of gene carrying have led to the search of a non-viral delivery system [1–4]. Among the non-viral systems, lipofection using cationic cholesterol derivatives is considered to be safer since it is less immunogenic and has low toxicity [5,6]. We reported that cationic nanoparticles (NPs) composed of cholesteryl-3β-carboxyamidoethylene-*N*-hydroxyethylamine (OH-Chol, Fig. 1) [5] and Tween 80 could deliver plasmid DNA into cells with high transfectional efficiency [7]. Cationic NPs bind electrostatically to negatively charged DNAs to form complexes called nanoplexes, which can enter the cells via endocytosis [8,9] followed by the escape from the endosomes into the cytoplasm and transfer into the nucleus [10].

In order to deliver DNAs efficiently to the nucleus and achieve high levels of expression, there are several obstacles that must be overcome even though they have successfully intruded into the cytoplasm [11,12]. We assumed that for the further development of more efficient NP vector, improvements have to be made to the processes of intracellular DNA delivery and intranucleus DNA transcription. Recently, it was reported that inhibition of histone deacetylase 6 (HDAC6) increased transfection efficiency due to the improved gene transfer in cytoplasm caused by hyperacetylation of microtubules [13]. It is also known that many kinds of HDAC inhibitors (HDACIs) augment the expression of genes because of the hyperacetylation of subnuclear core histone proteins. We therefore attempted to associate the function of NP with HDACI for the development of highly efficient vectors.

There are three different chemical types in major HDACIs, i.e. the fatty acid-type, benzamide-type and hydroxamate-type. Fatty acid-type HDACIs, such as butylate, or valproate [14], may have affinity to NPs, however, the HDACI activity of them is three orders of magnitude lower than the other types. Since, the benzamide-type HDACIs such as MS275 [15] and MGCD0103 [16] are selective inhibitor of class I HDACs, the improvement of DNA transport in the cytoplasm cannot be expected because the class II HDAC, namely HDAC6, may not be inhibited by them [17]. On the other hand, the hydroxamate-type HDACIs such as trichostatin A [18], suberoylanilide hydroxamic acid (SAHA, vorinostat) [19] and our K-series compounds [20–22] have potent inhibitory effects against broad HDAC isoenzymes, including cytoplasmic HDAC6 and nuclear

* Corresponding author. Tel.: +81 (0)6 6368 0884; fax: +81 (0)6 6388 8609.
E-mail address: ynagaoka@ipcku.kansai-u.ac.jp (Y. Nagaoka).

0223-5234/$ – see front matter © 2009 Elsevier Masson SAS. All rights reserved.
doi:10.1016/j.ejmech.2009.06.036

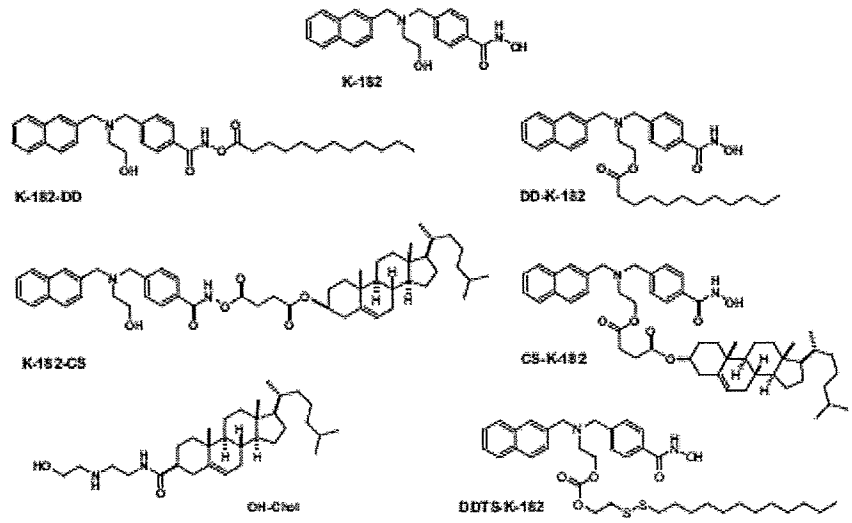

Fig. 1. Chemical structures of K-182, K-182 prodrugs and OH-Chol.

HDACI. We therefore assessed the compatibility of the hydroxamate-type HDACIs as a component of NP formulation. However, unsatisfactory results were obtained from admixed formulation of the HDACIs and NP, namely a considerable segregation of HDACIs occurred. Hence, we attempted to synthesize HDACI prodrugs compatible to NP. Taking into consideration the diverse derivatization, we selected one of the K-series compounds, K-182, (Fig. 1) [20] which has two OH groups to tether other groups with a biodegradable ester bond.

In this study, five kinds of K-182 prodrugs, DD–K-182, DDTS–K-182, CS–K-182, K-182–DD and K-182–CS, (Fig. 1) were synthesized to evaluate their compatibility to NP formulation and their ability to enhance the expression of the transfected genes.

2. Chemistry

We tried to form NPs containing hydroxamate-type HDACIs, but we decided against this because of the segregation of the compounds during preparation. To overcome this problem, we attempted to form HDACI prodrugs which have affinity to OH-Chol, the major component of NP. Regarding the activity and feasibility of derivatization, we selected K-182 as a substrate of the prodrugs.

K-182 has two hydroxyl (OH) groups that can link with other functional groups via ester bonds. We designed K-182 prodrugs in which K-182 is tethered to an aliphatic fatty acid or cholesteryl group via biodegradable bonds or linkers. When non-protected K-182 was treated with equimolar *n*-dodecanoic acid (lauric acid) with the coupling regent, DCC–DMAP, *n*-dodecanoic acid was selectively coupled to an OH group in hydroxamic acid to form mono-dodecanoate, K-182–DD, due to the higher acidity of OH in hydroxamic acid than in alcoholic OH in the hydroxyethyl group (Scheme 1). On the other hand, coupling of *n*-dodecanoic acid to a hydroxyethyl group was performed using a substrate in which OH in a hydroxamic acid was protected with tetrahydropyranyl ether (THP). After the coupling reaction, THP was deprotected with acetic acid in THF–H_2O at 60 °C for 10 h to give a monoester DD–K-182 with an excellent yield (Scheme 2). Two kinds of cholesteryl succinate monoesters of K-182, K-182–CS and CS–K-182, were synthesized by coupling cholesteryl succinate in the same manner as the coupling of *n*-dodecanoic acid (Scheme 2 and 3).

We also attempted to connect an aliphatic thiol to hydroxyethyl moiety in K-182 via a disulfide carbonate linker which is designed to release unmodified K-182 in the reductive cytosolic condition as shown in the route in Scheme 3 [23]. The mixed disulfide, (2-pyridinyldithio)ethyl carbonate **3**, for the subsequent coupling with aliphatic thiol was synthesized with the reaction of **1** and triphosgene, followed by condensation of 2-(2-pyridinyldithio) ethanol [24] to the acid chloride intermediate. Coupling of dodecanethiol to **3** followed by deprotection of THP afforded the target molecule DDTS–K-182 (Scheme 4). Accordingly, five kinds of K-182 prodrugs were prepared (Fig. 1).

3. Results and discussion

3.1. Optimization of concentration of K-182 prodrugs in NP and of concentration of the NPs in the medium affected to PC-3-Luc cells

In order to optimize the formulation, NPs containing K-182–DD with different proportions were prepared using the modified ethanol injection method as previously described [7] (Table 1). The

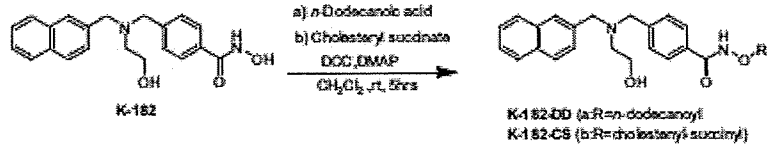

Scheme 1.

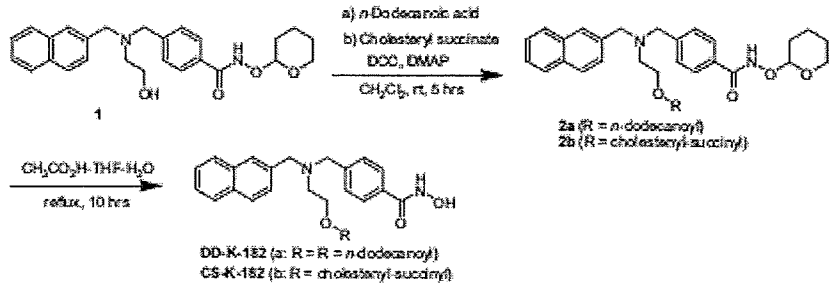

Scheme 2.

formulations were based on the original NP, yet 5, 10 or 20 mol% of OH-Chol in the original was displaced by K-182–DD (NP-5K, NP-10K and NP-20K, respectively). Subsequently, the resulting water suspension of the NPs (1 mg/mL) was incubated with plasmid DNAs for 10 min at room temperature to form nanoplexes (DNA/NP complexes). According to our previous study, the ratio between DNA and total NP is fixed so as to form nanoplexes at a charge ratio (+/−) of 3/1 of cationic NP to plasmid DNA pGL3-basic encoding luciferase gene without promoter, corresponding to a concentration ratio of NPs (μM) to DNA (μg/mL) of 10 throughout this experiment [25]. The nanoplexes were diluted with a cell growth medium to prepare the transfection medium containing 5, 10, 20 and 40 μM NPs with twofold serial dilution of the initial 40 μM NPs. In this optimization, PC-3 cells stably expressing *Gaussia* luciferase (PC-3-Gluc cells) were used to evaluate the effect of K-182–DD in each NP on the gene expression, excluding the factor of transfection. The cells were incubated with each medium for 24 or 48 h and the increased expression of the *Gluc* gene was evaluated using luciferase assay (Fig. 2).

Increased expression of the *Gluc* gene was observed significantly in the cells incubated with the medium containing 5–20 μM NP-10K and NP-20K both for 24 h and 48 h incubation times. (Fig. 2A and B) NP formulations of 40 μM, however, did not show the augmentation effect of K-182–DD, probably because of the higher cytotoxicity caused by higher concentration of OH-Chol and K-182–DD. Although 20 μM NP-20K seems optimum for the gene expression, the cytotoxicity in that condition was more significant (cell viability; 19.6 ± 1.4% of total cells as mean ± S.D.) compare to that of control NP or NP-10K (cell viability; 49.4 ± 2.2% and 34.3 ± 2.5%, respectively) at the same concentration ($P < 0.01$). We therefore chose the transfection media containing 20 μM NPs and we prepared NPs with 10 mol% of DD–K-182, CS–K-182, K-182–CS, and DDTS–K-182, as well as K-182–DD in further experiments. Their average particle sizes and ζ-potentials are in the range of 137.9–176.7 nm (polydispersity index; 0.1–0.2) and 64.0–63.0 mV, respectively and those of control NPs are 165.3 nm (polydispersity index; 0.02) and 48.8 mV, respectively. Replacement of 10 mol% of OH-Chol to K-182 prodrugs increased the surface potential of NPs, probably because of a tertiary amine, that can be positively charged, in K-182 moiety exposed on the surface of NPs.

3.2. Effect of K-182 prodrugs contained in NPs on expression of externally transfected genes

Nanoplexes were formed by the incubation of NPs with plasmid pCMV-Gluc control encoding secretable *Gaussia* luciferase (Gluc) under the control of the CMV promoter. According to the optimization mentioned above, nanoplexes were diluted to form the transfection medium of 20 μM NPs, containing 2 μM K-182 prodrugs at a charge ratio (+/−) of 3/1 of cationic NP to plasmid DNA, and were transfected to PC-3 cells. As shown in Fig. 3, NPs containing 10 mol% DD–K-182, K-182–DD and DDTS–K-182 (NP–DD–K-182, NP–K-182–DD and NP–DDTS–K-182) augmented the luciferase expression 2–3.5 times more than control NP. However, NPs containing 10 mol% cholesteryl ester, CS–K-182 and K-182–CS (NP–CS–K-182 and NP–K-182–CS) did not increase the expression. It is interesting that the addition of 2 μM K-182 to the medium containing control NP did not potentiate the expression of transfected genes. Similar results were obtained when Sk-Br-3 cells were used as a host for the transfection with NP–DD–K-182, NP–K-182–DD and NP–DDTS–K-182, i.e. they enhanced the expression about three times more than control NP. The addition of external K-182 did not increase the expression, in these cells. The simultaneous incorporation of DNA and K-182 prodrugs into the cells with NPs will be critical for the activation of gene expression.

3.3. Effect of NPs composed of K-182 prodrugs on acetylation of histone H3 in human prostate tumor PC-3 cells

Histone H3 is one of the core histone proteins in the chromatin of eukaryotic cells. Hyperacetylation of lysine residues, i.e. lysine 9, in the N-terminal tails of histone H3 loosens the histone–DNA binding and activates gene transcription. On the other hand, deacetylation of acetylated lysine residues leads to tight histone–DNA binding, which restricts the access of transcriptional factors. Histone acetyltransferases (HATs) and HDACs play a crucial role in this reversible acetylation and deacetylation of histones regulating gene expression. Inhibition of HDACs, therefore, induces histone hyperacetylation and activates gene transcription [26–28].

Prior to examine the acetylation of cellular histone H3, we tested the effect of intact K-182 prodrugs, K-182–DD, DD–K-182 and

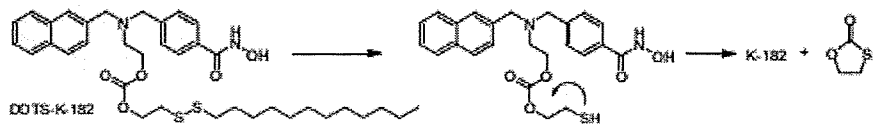

Scheme 3. Disulfide mediated release of K-182 from the carbonate linker.

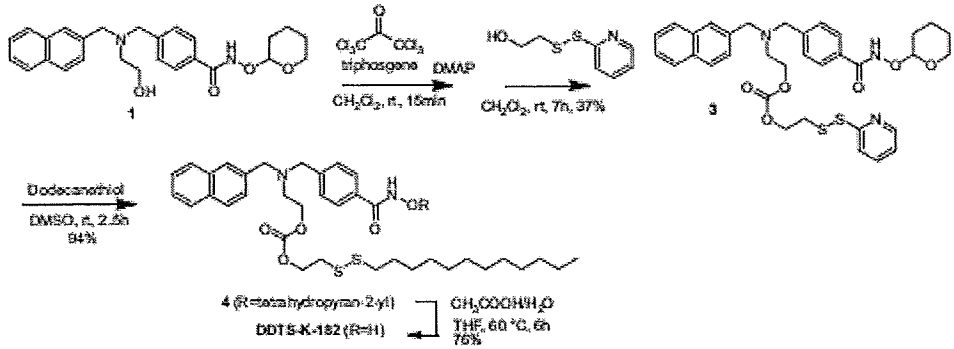

Scheme 4.

DDTS–K-182 on HDAC activity. As shown in Table 2, K-182 prodrugs are inactive (IC_{50} > 10 μM), although K-182 exhibited IC_{50} of 0.90 μM. The activity of HDACI was recovered when DDTS–K-182 was treated with dithiothreitol, indicating the release of K-182 by degradation of disulfide carbonate linker with reductive conditions.

We tested the effect of nanoplexes containing K-182 prodrugs on the acetylation of core histone H3 protein in human prostate tumor cells, PC-3, using western blot analysis detecting the acetylation on Lys-9 side chains. Incubation of the cells with nanoplexes formed with NP–DDTS–K-182, NP–DD–K-182 or NP–K-182–DD resulted in increased levels of acetylated histone H3 protein in the cells to a similar extent as those increased with 2 μM K-182 or another type of HDACI K-32 [22] in the medium with or without the presence of NP–pGL3-basic nanoplexes (Fig. 4). This observation, together with the result that intact prodrugs are inactive in HDAC inhibition, suggesting that free K-182 is efficiently released from the complexes of prodrugs in the cells and inhibits HDAC in the nucleus resulting in the hyperacetylation of histone H3.

It remains controversial that addition of K-182 externally to the medium did not increase the expression of transfected genes in PC-3 cells as shown in Fig. 3, even though the hyperacetylation of histone H3 in the cells was observed in the similar condition (Fig. 4) and the fact that addition of K-182 to PC-3-Gluc cells, on the other hand, increased the expression of *Gluc* gene stably expressed in the cells (Fig. 5). The simultaneous delivery of K-182 prodrugs and genes into the cells with the formulation of nanoplexes is probably important to enhance the outer gene expression.

4. Conclusion

In conclusion, cationic NPs composed of 10 mol% K-182 prodrugs, K-182–DD, DD–K-182 and DDTS–K-182, with 85 mol% OH-Chol and 5 mol% Tween 80 were prepared as a DNA vector to transfect plasmid DNA into human prostate cancer cells, PC-3, or human breast cancer cells, Sk-Br-3. These NPs exhibited expression of the genes two to four times more efficiently than those with the original NP. The enhancement of the gene expression will be due to the hyperacetylation of core histones caused by K-182 derived from K-182 prodrugs in the NP formulation.

Table 1
Formulae of NPs containing K-182–DD.

NP formulation[a]	Components (mol%)		
	OH-Chol	Tween 80	K-182–DD
Control NP	95	5	0
NP-5K	90	5	5
NP-10K	85	5	10
NP-20K	75	5	20

[a] NPs were prepared with a cationic cholesterol (OH-Chol), Tween 80 and K-182–DD using modified ethanol injection method [7] as 1 mg/mL suspension in water.

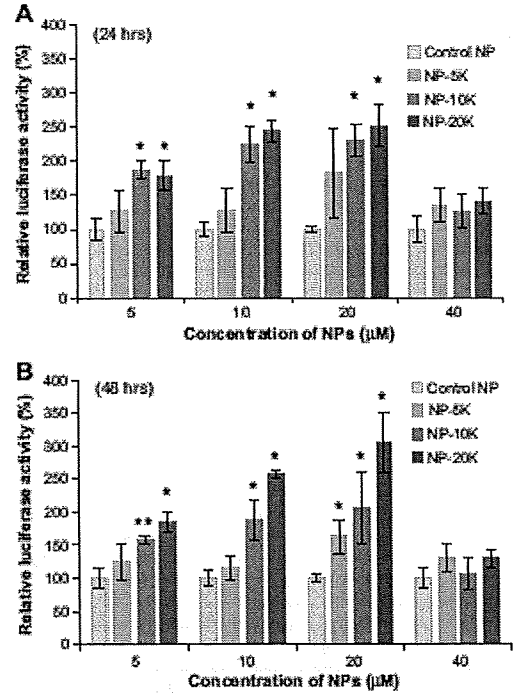

Fig. 2. Effect of concentration of K-182–DD in NPs on increased expression of *Gluc* gene stably expressed in PC-3-Gluc cells at a charge ratio (+/−) of 3/1 of cationic NP to plasmid DNA (corresponding to a concentration ratio of NPs (μM) to DNA (μg/mL) of 10). PC-3-Gluc cells were incubated for 24 h (A) or 48 h (B) with cell growth media containing nanoplexes formed with 5, 10 and 20 mol% K-182–DD in NPs; NP-5K, NP-10K or NP-20K. Each column represents the mean ± S.D. ($n = 3$). *$P < 0.05$, significantly different from control.

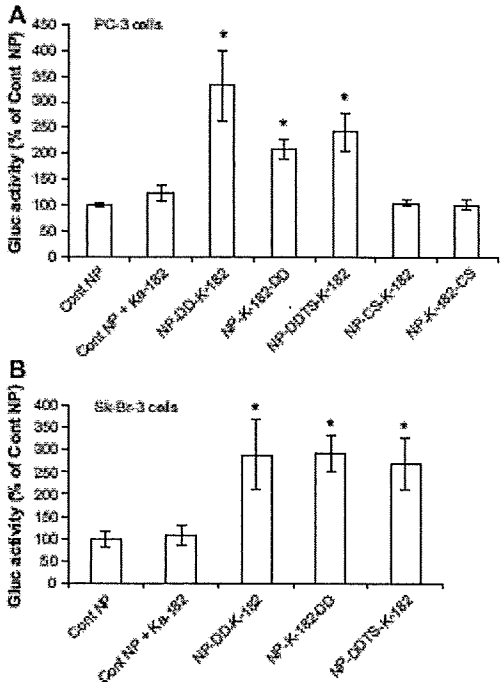

Fig. 3. Effects of 10 mol% K-182 prodrugs contained in NPs on the expression of genes transfected to PC-3 cells (A) and Sk-Br-3 cells (B). PC-3 cells or Sk-Br-3 cells were incubated for 24 h in the transfection medium containing nanoplexes formed with 20 μM NPs and 2 μg/mL plasmid DNA, pCMV-Gluc. For the control, the media containing or not containing 2 μM K-182 were used for transfection with the control NP. Each column represents the mean ± S.D. ($n = 3$). $^{*}P < 0.01$, significantly different from control.

5. Experimental

5.1. Synthesis of K-182 prodrugs

Melting points were determined on a Yanagimoto MP-32 micromelting point apparatus and are uncorrected. IR spectra were recorded on Shimadzu FTIR-8400 infrared spectrophotometer. FAB-MS spectra were measured on a JEOL JMS-HX 100 instrument. ^{1}H and ^{13}C NMR spectra are recorded on JEOL EX-400 (399.7 MHz for ^{1}H NMR and 100.4 MHz for ^{13}C NMR) instruments using tetramethylsilane as an internal standard. Analytical and preparative TLC were performed using Silica gel 60 F254 (Merck, 0.25 and 0.5 mm, respectively) glass plates. Column chromatography was performed using Silica Gel 60 (70–230 mesh ASTM).

Table 2
Inhibitory effect of HDACIs and K-182 prodrugs on HDAC.

Compounds	IC_{50} (μM)[a,b]
TSA[c]	0.012
K-182	0.90
K-182–DD	>10
DD–K-182	>10
DDTS–K-182	>10
DDTS–K-182 + DTT[d]	2.7

[a] Inhibition of crude HDACs from nuclear extract of Hela cells provided in Cyclex HDAC Assay Kit.
[b] Assays were performed in duplicate.
[c] Trichostatin A (TSA) as positive control of HDACI.
[d] DDTS–K-182 was preincubated with equimolar dithiothreitol (DTT) in DMSO for 2 h before addition to the assay buffer.

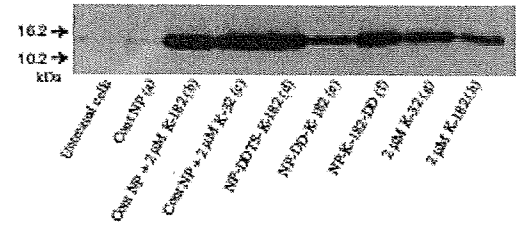

Fig. 4. Acetylation of core histone H3 protein in PC-3 cells induced by HDACIs (K-2F and K-182) and NPs composed of K-182 prodrugs. The cells were treated with a medium containing (a–f) or not containing (g, h) NP–pG13-basic nanoplexes in the presence (b–h) or absence (a) of the HDACIs. The medium containing the nanoplexes (a–f) was formed with pG13-basic plasmid DNA (2 μg/mL) and 20 μM NP (a–c), NP-DDTS–K-182 (d), NP-DD–K-182 (e) or NP-K-182–DD (f). After 24 h incubation of the medium, cellular proteins were isolated from the cells and were resolved on a 12% SDS–PAGE (each 3 μg protein in a well), followed by Western blot analysis for acetylated histone H3 protein.

5.1.1. N-(Dodecanoyloxy)-4-{[(2-hydroxyethyl)(2-naphthylmethyl)-amino]methyl}benzamide (K-182–DD)

To a solution of K-182 (33.2 mg, 94.6 μmol) in CH_2Cl_2 (4.0 mL) were added n-dodecanoic acid (19.0 mg, 94.6 μmol), DCC (19.5 mg 94.6 μmol) and DMAP (11.6 mg, 94.6 μmol). After being stirred for 5 h at rt, the precipitate was filtered off and the filtrate was concentrated in vacuo. Purification of the resulting residue by silica gel column chromatography (eluent: ethylacetate/hexane = 1/1) gave K-182–DD (12.2 mg, 23.0 μmol, 24.3% yield) as a colorless oil. IR ($CHCl_3$) γ/cm^{-1}: 3341, 3010, 2927, 2854, 1780, 1697, 14,111, 1141, 773; ^{1}H NMR ($CDCl_3$) δ: 0.88 (t, 3H, $J = 7.2$ Hz, CH_3CH_2), 1.0–1.4 (m, 16H, $-(CH_2)_8-$), 1.60–1.75 (m, 2H, $COCH_2CH_2$), 2.55 (t, 2H, $J = 7.6$ Hz, $COCH_2$), 2.71 (t, 2H, $J = 5.2$ Hz, NCH_2CH_2), 3.62 (t, 2H, $J = 5.2$ Hz, $HOCH_2CH_2$), 3.70 (s, 2H, NCH_2–naph), 3.78 (s, 2H, NCH_2Ph), 7.41–7.52 (m, 5H, Ar–H), 7.71–7.84 (m, 6H, Ar–H); ^{13}C NMR ($CDCl_3$) δ: 14.10, 22.66, 24.70, 24.90, 25.59, 28.99, 29.14, 29.31, 29.37, 29.56,

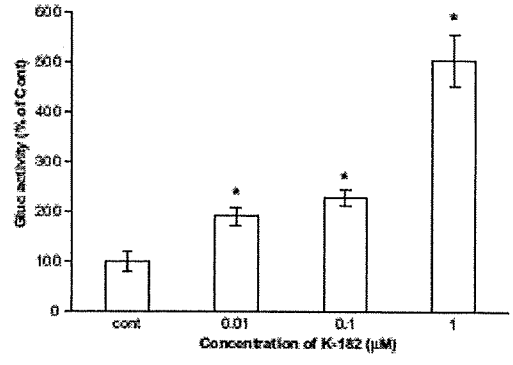

Fig. 5. Effect of K-182 on the expression of genes stably expressed in PC-3-Gluc cells. PC-3-Gluc cells were incubated for 24 h with cell growth media with or without K-182. Each column represents the mean ± S.D. ($n = 3$). $^{*}P < 0.01$, significantly different from control.

31.78, 31.89, 33.90, 55.11, 58.03, 58.61, 58.77, 125.85, 126.19, 126.86, 127.63, 127.67, 127.71, 127.80, 128.37, 129.29, 129.78, 132.84, 133.29, 135.86, 144.22, 172.20; HR-FAB-MS *m/z*: 533.3370 (calcd for $C_{33}H_{45}N_2O_4$, 533.3379).

5.1.2. Cholest-5-en-3-yl 4-{[(4-{[(2-hydroxyethyl)(2-naphthylmethyl)amino]methyl}benzoyl) amino]oxy}-4-oxobutanoate (K-182–CS)

To a solution of K-182 (21.2 mg, 60.5 μmol) in CH_2Cl_2 (2.0 mL) were added cholesteryl succinate (29.5 mg, 60.5 μmol), DCC (12.5 mg, 60.5 μmol) and DMAP (7.4 mg, 60.5 μmol). After being stirred for 6 h at rt, the precipitate was filtered off and the filtrate was concentrated in vacuo. Purification of the resulting residue by preparative SiO_2 TLC (eluent: ethylacetate/hexane = 4/5) gave K-182–CS (10.5 mg, 12.8 μmol, 21.2% yield) as a colorless oil. IR ($CHCl_3$) γ/cm^{-1}: 3320, 2949, 2868, 1759, 1724, 1466, 1364, 1105, 667; ^{1}H NMR ($CDCl_3$) δ: 0.67 (s, 3H, 18′-CH_3), 0.85 (d, 3H, J = 1.6 Hz, 26′ or 27′-CH_3), 0.87 (d, 3H, J = 1.6 Hz, 26′ or 27′-CH_3), 0.90–2.05 (m, 26H), 0.91 (d, 3H, J = 6.4 Hz, 21′-CH_3), 1.01 (s, 3H, 19′-CH_3), 2.32 (d, 2H, J = 7.6 Hz, 4′-CH_2), 2.71 (m, 4H, $COCH_2CH_2CO$), 2.87 (t, 2H, J = 6.8 Hz, NCH_2CH_2), 3.62 (t, 2H, J = 5.6 Hz, $HOCH_2CH_2$), 3.70 (s, 2H, NCH_2–naph), 3.78 (s, 2H, NCH_2–Ph), 4.63 (m, 1H, 3′-CH), 5.36 (m, 1H, 6′-CH=C), 7.41–7.48 (m, 5H, Ar–H), 7.70–7.83 (m, 6H, Ar–H); ^{13}C NMR ($CDCl_3$) δ: 11.85, 18.70, 19.28, 21.02, 22.54, 22.80, 23.83, 24.27, 27.05, 27.69, 28.00, 28.21, 29.14, 31.84, 31.89, 35.78, 36.18, 36.58, 36.94, 38.00, 39.52, 39.73, 42.32, 50.01, 55.17, 56.16, 56.69, 58.07, 58.65, 58.82, 74.79, 122.77, 125.84, 126.19, 126.87, 127.64, 127.68, 127.71, 127.79, 128.36, 129.29, 129.61, 132.86, 133.30, 135.87, 139.49, 144.29, 171.06; HR-FAB-MS *m/z*: 819.5320 (calcd for $C_{52}H_{71}N_2O_6$, 819.5234).

5.1.3. 4-{[(2-Hydroxyethyl)(2-naphthylmethyl)amino]methyl}-N-(tetrahydro-2H-pyran-2-yloxy) benzamide (1)

To a mixture of 4-{[(2-naphthylmethyl)amino]methyl}-*N*-(tetrahydro-2*H*-pyran-2-yloxy) benzamide [20] (1.0 g, 0.94 mmol) and Et_3N 0.71 mL (5.12 mmol) in CH_3CN (20 mL) was added 2-bromoethanol (0.36 mL, 5.12 mmol). After stirring for 6 h at 60 °C, the mixture was evaporated to remove the solvent. Purification of the resulting residue by SiO_2 column chromatography (eluent: ethylacetate/hexane = 3/2) gave **1** as colorless amorphous (650 mg, 58.5% yield). IR (KBr) γ/cm^{-1}: 3221, 2936, 1719, 1653, 1275, 1204, 1051, 905; ^{1}H NMR ($CDCl_3$) δ: 1.62–1.86 (6H, m, $CH_2 \times 3$ of THP), 2.71 (2H, t, J = 5.6 Hz, N–CH_2–CH_2), 3.62 (2H, t, J = 5.6 Hz, CH_2–CH_2–OH), 3.64–3.68 (1H, m, –CH_a–O of THP), 3.69 (2H, s, N–CH_2–Ar), 3.78 (2H, s, naph–CH_2–N), 4.00 (1H, ddd, J = 11.2, 9.2, 2.8 Hz, –CH_b–O of THP) 5.07 (1H, t, J = 2.8 Hz, O–CH–O of THP), 7.38–7.84 (11H, m, Ar–H), 8.81 (1H, s, CO–NH–O); ^{13}C NMR ($CDCl_3$) δ: 18.61, 24.99, 28.03, 54.98, 57.97, 58.54, 58.71, 62.63, 102.65, 125.79, 126.14, 126.83, 127.37, 127.59, 127.67, 127.73, 128.29, 129.09, 130.97, 132.79, 133.24, 135.91, 143.33; HR-FAB-MS *m/z*: 435.2289 (calcd for $C_{26}H_{31}N_2O_4$, 435.2284).

5.1.4. 2-[(2-Naphthylmethyl)(4-{[(tetrahydro-2H-pyran-2-yloxy)amino]carbonyl}benzyl)amino] ethyl laurate (2a)

To a solution of **1** (26.2 mg, 60.3 μmol) in CH_2Cl_2 (2.0 mL) were added *n*-dodecanoic acid (12.1 mg, 60.3 μmol), *N,N*-dicyclohexylcarbodiamide (DCC) (12.4 mg, 60.3 μmol) and *N,N*-dimethyl-4-aminopyridine (DMAP) (7.37 mg, 60.3 μmol). After being stirred for 5 h at rt, the precipitate was filtered off and the filtrate was concentrated in vacuo. Purification of the resulting residue by silica gel column chromatography (eluent: ethylacetate/hexane = 1/4) gave **2a** (22.4 mg, 36.3 μmol, 60.2% yield) as a colorless oil. IR ($CHCl_3$) γ/cm^{-1}: 3010, 2927, 1728, 1683, 1456, 1112, 777, 669; ^{1}H NMR ($CDCl_3$) δ: 0.87 (t, 3H, J = 7.2 Hz, –CH_2CH_3), 1.25–1.28 (m, 16H, –$(CH_2)_8$–), 1.43–1.58 (m, 6H), 1.84–1.92 (m, 2H, $COCH_2CH_2$), 2.28 (t, 2H, J = 7.6 Hz, $COCH_2$), 2.77 (t, 2H, J = 5.6 Hz, NCH_2CH_2), 3.64–3.68 (1H, m, –CH_a–O of THP), 3.72 (s, 2H, NCH_2Ph), 3.78 (s, 2H, NCH_2), 3.95–4.10 (m, 1H, –CH_b–O of THP), 4.20 (t, 2H, J = 6.0 Hz, OCH_2CH_2N), 5.08 (m, 1H, OCHO), 7.43–7.52 (m, 5H, Ar–H), 7.70–7.83 (m, 6H, Ar–H); ^{13}C NMR ($CDCl_3$) δ: 14.09, 18.66, 22.66, 24.91, 25.02, 25.60, 28.05, 29.18 29.28, 29.31, 29.46, 29.59, 31.86, 33.91, 34.34, 51.91, 58.31, 58.89, 62.05, 62.69, 102.71, 125.62, 126.00, 126.92, 127.20, 127.30, 127.61, 127.65, 128.01, 128.88, 130.75, 132.80, 133.27, 136.56, 144.06, 173.74; HR-FAB-MS *m/z*: 617.3960 (calcd for $C_{38}H_{53}N_2O_5$, 617.3954).

5.1.5. 1-Cholest-5-en-3-yl 4-{2-[(2-naphthylmethyl)(4-{[(tetrahydro-2H-pyran-2-yloxy) amino]carbonyl}benzyl)amino]ethyl} succinate (2b)

To a solution of **1** (48.6 mg, 112 μmol) in CH_2Cl_2 (2.0 mL) were added cholesteryl succinate (54.4 mg, 112 μmol), DCC (23.0 mg, 111.6 μmol) and DMAP (13.6 mg, 111.6 μmol). After being stirred for 4 h at rt, the precipitate was filtered off and the filtrate was concentrated in vacuo. Purification of the resulting residue by preparative SiO_2 TLC (eluent: ethylacetate/hexane = 1/2) gave **2b** (66.3 mg, 73.4 μmol, 65.8% yield) as a colorless oil. IR ($CHCl_3$) γ/cm^{-1}: 3008, 2947, 2854, 1728, 1683, 1456, 1363, 1112, 761; ^{1}H NMR ($CDCl_3$) δ: 0.67 (s, 3H, 18′-CH_3), 0.85 (d, 3H, J = 1.6 Hz, 26′ or 27′-CH_3), 0.87 (d, 3H, J = 1.6 Hz, 26′ or 27′-CH_3), 0.9–2.1 (m, 32H), 0.91 (d, 3H, J = 6.4 Hz, 21′-CH_3), 1.01 (s, 3H, 19′-CH_3), 2.30 (d, 2H, J = 8.0 Hz, 4′-CH_2), 2.57 (m, 4H, $COCH_2CH_2CO$), 2.76 (t, 2H, J = 5.6 Hz, NCH_2CH_2), 3.63–3.67 (1H, m, –CH_a–O of THP), 3.69 (s, 2H, NCH_2Ph), 3.78 (s, 2H, NCH_2), 3.95–4.10 (m, 1H, –CH_b–O of THP), 4.20 (t, 2H, J = 5.6 Hz, OCH_2CH_2N), 4.62 (m, 1H, 3′-CH), 5.08 (m, 1H, OCHO of THP), 5.35 (s, 1H, 6′-CH=C), 7.43–7.53 (m, 5H, Ar–H), 7.70–7.82 (m, 6H, Ar–H); ^{13}C NMR ($CDCl_3$) δ: 11.83, 18.63, 18.70, 19.27, 21.00, 22.54, 22.80, 23.81, 24.26, 24.91, 25.04, 25.60, 27.71, 27.99, 28.07, 28.21, 29.41, 31.83, 31.88, 33.91, 35.76, 36.17, 36.55, 36.92, 38.04, 39.50, 39.71, 42.29, 49.99, 51.96, 56.12, 56.67, 58.31, 59.01, 62.44, 62.61, 74.43, 102.63, 122.71, 125.63, 126.02, 126.94, 127.24, 127.34, 127.62, 127.66, 128.06, 128.87, 130.82, 132.81, 133.27, 136.52, 144.01, 171.34, 172.17; HR-FAB-MS *m/z*: 903.5882 (calcd for $C_{57}H_{79}N_2O_7$, 903.5887).

5.1.6. 2-[(4-{(Hydroxyamino)carbonyl}benzyl)(2-naphthylmethyl)amino]ethyl laurate (DD-K-182)

To a solution of **2a** (16.5 mg, 26.8 μmol) in THF (1.0 mL) were added acetic acid (2.0 mL) and H_2O (0.5 mL). After refluxing for 10 h, the solution was concentrated in vacuo. Purification of the residue by preparative SiO_2 TLC (eluent: ethylacetate/hexane = 1/2) gave DD-K-182 (11.5 mg, 21.6 μmol, 80.6% yield) as a brownish oil. IR ($CHCl_3$) γ/cm^{-1}: 3405, 3210, 2927, 2854, 1728, 1612, 1454, 763; ^{1}H NMR ($CDCl_3$) δ: 0.87 (t, 3H, J = 6.8 Hz, –CH_2CH_3), 1.03–1.25 (m, 16H, –$(CH_2)_8$–), 1.57–1.70 (m, 2H, $COCH_2CH_2$), 2.27 (t, 2H, J = 7.6 Hz, $COCH_2$), 2.76 (t, 2H, J = 5.6 Hz, NCH_2CH_2O), 3.70 (s, 2H, naph–CH_2N), 3.78 (s, 2H, NCH_2–Ph), 4.18 (t, 2H, J = 5.6 Hz, NCH_2CH_2O), 7.42–7.50 (m, 5H, Ar–H), 7.68–7.82 (m, 6H, Ar–H); ^{13}C NMR ($CDCl_3$) δ: 14.09, 22.66, 24.90, 24.93, 25.58, 29.18, 29.28, 29.32, 29.46, 29.60, 31.89, 33.87, 34.36, 52.04, 58.36, 59.00, 62.08, 125.66, 126.03, 126.87, 126.92, 127.34, 127.62, 127.66, 128.04, 129.01, 129.37, 132.83, 133.30, 136.54, 144.41, 173.78; HR-FAB-MS *m/z*: 533.3373 (calcd for $C_{33}H_{45}N_2O_4$, 533.3379).

5.1.7. 1-Cholest-5-en-3-yl 4-{2-[(4-{[(hydroxyamino) carbonyl]benzyl}(2-naphthylmethyl) amino]ethyl} succinate (CS-K-182)

To a solution of **2b** (33.0 mg, 36.6 μmol) in THF (1.0 mL) were added acetic acid (2.0 mL) and H_2O (0.5 mL). After refluxing for 7 h, the solution was concentrated in vacuo. Purification of the residue by preparative SiO_2 TLC (eluent: ethylacetate/hexane = 2/3) gave CS-K-182 (18.4 mg, 22.5 μmol, 61.5% yield) as a brownish oil. IR ($CHCl_3$) γ/cm^{-1}: 3421, 2935, 2854, 1728, 1612, 1465, 1365, 1164; ^{1}H

NMR ($CDCl_3$) δ: 0.87 (s, 3H, 18′-CH_3), 0.85 (d, 3H, J = 1.6 Hz, 26′ or 27′-CH_3), 0.87 (d, 3H, J = 1.6 Hz, 26′ or 27′-CH_3), 0.9–2.1 (m, 26H), 0.91 (d, 3H, J = 6.4 Hz, 21′-CH_3), 1.01 (s, 3H, 19′-CH_3), 2.30 (m, 2H, 4′-CH_2), 2.56 (m, 4H, $COCH_2CH_2CO$), 2.74 (m, 2H, NCH_2CH_2), 3.68(s, 2H, NCH_2–naph), 3.80 (s, 2H, NCH_2Ph), 4.19 (t, 2H, J = 4.8 Hz, OCH_2CH_2N), 4.61 (m, 1H, 3′-CH), 5.34 (s, 1H, 6′-CH=C), 7.44–7.54 (m, 5H) 7.69–7.80 (m, 6H); ^{13}C NMR ($CDCl_3$) δ: 11.85, 18.71, 19.28, 21.02, 22.55, 22.80, 23.83, 24.27, 27.72, 28.00, 28.21, 29.18, 29.41, 29.68, 31.85, 31.88, 35.78, 36.19, 36.56, 36.91, 38.03, 39.52, 39.72, 42.32, 49.98, 52.22, 56.15, 56.67, 58.37, 59.26, 62.42, 74.64, 122.77, 125.68, 126.05, 126.94, 127.39, 127.63, 127.67, 128.09, 128.97, 132.84, 133.300, 136.50, 139.50, 144.36, 171.99, 172.15; HR-FAB-MS m/z: 819.5304 (calcd for $C_{52}H_{71}N_2O_6$, 819.5234).

5.1.8. 2-[(2-Naphthylmethyl)(4-{[(tetrahydro-2H-pyran-2-yl)oxy]amino}carbonyl)benzyl]amino} ethyl 2-(2-pyridinyldisulfanyl)ethyl carbonate (3)

To a solution of **1** (100 mg, 0.230 mmol) in CH_2Cl_2 (2.0 mL) were added DMAP (167 mg, 1.38 mmol) and triphosgene (23.9 mg, 0.0805 mmol). After being stirred for 15 min at rt, to the solution was added 2-(2-pyridinyldisulfanyl)ethanol [24,29] (43.0 mg, 0.230 mmol) and the solution was stirred for another 7 h at rt. The reaction mixture was diluted with $CHCl_3$ (20 mL), washed with water, dried over Na_2SO_4 and concentrated in vacuo. Purification of the resulting residue by preparative SiO_2 TLC (eluent: ethylacetate/hexane = 3/2) gave **3** (55.0 mg, 36.9% yield) as a colorless oil. IR (neat) γ/cm^{-1}: 3400, 3027, 3010, 2950, 2824, 1743, 1684, 703; ^1H NMR ($CDCl_3$) δ: 1.60–1.86 (m, 6H, CH_2 × 3 of THP), 2.79 (t, 2H, J = 6 Hz, CH_2CH_2–SS), 3.05 (t, 2H, J = 3.2 Hz, NCH_2CH_2), 3.64 (m, 1H, –CH_a–O of THP), 3.72 (s, 2H, NCH_2–naph), 3.80 (s, 2H, $PhCH_2N$), 3.99 (ddd, 1H, J = 11.2, 9.2, 2.8 Hz, –CH_b–O of THP), 4.23 (t, 2H, J = 3.2 Hz, CH_2CH_2OCO), 4.35 (t, 2H, J = 6.0 Hz, OCOO–CH_2–CH_2), 5.08 (m, 1H, OCHO of THP), 7.07–7.81 (m, 15H, Ar–H), 8.45 (m, 1H, Ar–H); ^{13}C NMR ($CDCl_3$) δ: 18.65, 24.99, 28.07, 37.00, 51.79, 58.33, 58.86, 62.61, 65.34, 65.84, 76.68, 77.00, 77.31, 102.60, 119.88, 120.88, 125.63, 125.99, 126.87, 127.24, 127.32, 127.62, 128.04, 128.82 132.78, 133.25, 136.32, 137.05, 143.73, 149.68, 154.76, 159.47; HR-FAB-MS m/z: 648.2205 (calcd for $C_{34}H_{38}N_3O_6S_2$ [M + H^+], 648.2202).

5.1.9. 2-(Dodecyldisulfanyl)ethyl 2-[(2-naphthylmethyl)(4-{[(tetrahydro-2H-pyran-2-yl)oxy]amino}carbonyl)benzyl]amino}ethyl carbonate (4)

To a solution of **3** (55 mg, 0.085 mmol) in DMSO (1.5 mL) was added dodecanethiol (0.02 mL, 0.085 mmol). After being stirred for 2.5 h at rt, the reaction mixture was diluted with $CHCl_3$ (10 mL), washed with water, dried over Na_2SO_4 and concentrated in vacuo. Purification of the resulting residue by preparative SiO_2 TLC (eluent: ethylacetate/hexane = 3/2) gave **4** (59.0 mg, 93.9% yield) as a colorless oil. IR (neat) γ/cm^{-1}: 3400, 3030, 2927, 2855, 1744, 1683; ^1H NMR ($CDCl_3$) δ: 0.88(3H, t, J = 7.2 Hz, $CH_3(CH_2)_9CH_3$) 1.15–1.35 (18H, m, $CH_2(CH_2)_2CH_3$), 1.35 (2H, t, J = 7.2 Hz, $CH_2(CH_2)_9CH_3$), 1.62–1.86 (6H, m, CH_2 × 3 of THP), 2.69 (2H, t, J = 7.2 Hz, SS–$CH_2CH_2(CH_2)_9CH_3$), 2.81 (2H, t, J = 6.8 Hz, N–CH_2–CH_2), 2.90 (2H, t, J = 6.8 Hz, OCH_2CH_2–SS), 3.64 (1H, m, CH_2CH_a–O of THP), 3.73 (2H, s, NCH_2–naph), 3.80 (2H, s, naph–CH_2N), 4.00 (1H, ddd, J = 11.2, 9.2, 2.8 Hz, CH_2CH_b–O of THP), 4.25 (2H, t, J = 6.0 Hz, NCH_2CH_2–OCO), 4.34 (2H, t, J = 6.8 Hz, $COOCH_2CH_2S$), 5.07 (1H, m, OCHO of THP), 7.45–7.93 (11H, m, Ar–H); ^{13}C NMR ($CDCl_3$) δ: 14.05, 18.68, 22.63, 24.99, 28.06, 28.46, 29.09, 29.16, 29.28, 29.44, 29.53, 29.58, 31.86, 36.82, 39.09, 39.19, 41.18, 51.82, 58.35, 58.91, 60.35, 62.70, 65.81, 65.87, 76.68, 77.00, 77.31, 102.72, 125.61, 125.98, 126.86, 127.22, 127.32, 127.62, 128.04, 128.58, 128.87, 129.71, 130.78, 132.80, 133.27, 136.34, 143.83, 154.87. HR-FAB-MS m/z: 738.3816 (calcd for $C_{41}H_{59}N_3O_6S_2$ [M + H^+], 739.3815).

5.1.10. 2-(Dodecyldisulfanyl)ethyl 2-[(4-[(hydroxyamino)carbonyl]-benzyl)(2-naphthylmethyl) amino]ethyl carbonate (DDTS-K-182)

To a solution of **4** (29.0 mg, 39.0 μmol) in THF (0.4 mL) were added acetic acid (0.8 mL) and H_2O (0.2 mL). After refluxing for 6 h, the solution was concentrated in vacuo. Purification of the residue by preparative SiO_2 TLC (eluent: ethylacetate/hexane = 1/2) gave DDTS-K-182 (19.0 mg, 76.0% yield) as a brownish oil. IR (neat) γ/cm^{-1}: 3300, 3026, 2928, 2855, 1730, 1653, 705; ^1H NMR ($CDCl_3$) δ: 0.88 (t, 3H, J = 7.2 Hz, $CH_2(CH_2)_{10}CH_3$), 1.15–1.45 (m, 20H, $CH_2(CH_2)_{10}CH_3$), 2.69 (t, 2H, J = 7.2 Hz, SS–$CH_2(CH_2)_{10}CH_3$), 2.81 (t, 2H, J = 5.2 Hz, NCH_2CH_2O), 2.90 (t, 2H, J = 5.6 Hz, OCH_2CH_2–SS), 3.73 (s, 2H, NCH_2–naph), 3.80 (s, 2H, $PhCH_2N$), 4.24 (t, 2H, J = 5.2 Hz, NCH_2CH_2OCO), 4.34 (t, 2H, J = 5.6 Hz, OCH_2CH_2–SS), 7.47–7.81 (m, 11H, Ar–H); ^{13}C NMR ($CDCl_3$) δ: 14.06, 14.14, 20.99, 22.64, 28.47, 29.10, 29.18, 29.30, 29.46, 29.55, 29.59, 29.80, 29.65, 31.88, 36.82, 39.20, 51.91, 58.39, 59.03, 60.41, 65.83, 65.90, 125.66, 126.02, 126.87, 127.37, 127.63, 128.07, 128.99, 132.82, 133.28, 136.32, 144.05, 154.91; HR-FAB-MS m/z: 654.3243 (calcd for $C_{36}H_{51}N_3O_5S_2$ [M + H^+], 6553239).

5.2. Preparation of nanoparticles and nanoplexes

OH-Chol was synthesized as previously described [7]. Tween 80 was obtained from NOF Co. Ltd. (Tokyo, Japan). NPs were prepared by a modified ethanol injection method as previously described [7]. For example, in the case of NP–K-182–DD, OH-Chol:Tween 80:K-182–DD = 85:5:10 molar ratio (=10:1.42:1.17, weight) was dissolved in about 5 mL of ethanol, then the ethanol was removed with a rotary evaporator till 1–2 mL was left. Next, a constant volume of water was added to the ethanol solution. NPs formed instantly after further evaporation of the residual ethanol. The concentration of OH-Chol was adjusted to 1 mg/mL in the final NP suspension with drop of water. Then the nanoparticle suspension was filtered through 0.45-μm Millex-HA filters (Millipore, Cork, Ireland) to sterilize it. The particle size distributions were measured by the dynamic light scattering method (ELS-Z2, Otsuka Electronics Co., Ltd., Osaka, Japan), at 25 °C after the dispersion was diluted to an appropriate volume with water.

5.3. Cell culture

PC-3 cells were supplied by the Cell Resource Center for Biomedical Research, Tohoku University (Miyagi, Japan). The cells were grown in RPMI-1640 medium (Invitrogen, Carlsbad, CA, USA) supplemented with 10% heat-inactivated fetal bovine serum (FBS) (Invitrogen) and kanamycin (100 μg/mL) at 37 °C in a 5% CO_2 humidified atmosphere.

For the preparation of PC-3 cells stably expressing *Gaussia* luciferase (Gluc), PC-3 cells were plated on 35-mm culture dishes. Twenty-four hours later, the cells were transfected with 2 μg of pCMV-Gluc (New England Biolabs, MA, USA) using lipofectamine 2000 reagents (Invitrogen). The transfected cells were selected in medium with 800 μg/mL G418 sulfate for 2 weeks. G418-resistant colonies were subcultured and established as a permanent cell line transduced with pCMV-Gluc (PC-3-Gluc) and were used for subsequent experiments.

5.4. Transfection

Based on a preliminary experiment [25], the optimized ratio (+/−) of cationic lipid to plasmid DNA was determined as 3:1. The nanoplex at a charge ratio (+/−) of 3/1 was formed by addition of each NP (9.5 μL) to plasmid DNA with gentle shaking and leaving at room temperature for 10 min. for transfection, each nanoplex was

diluted in 1 mL of medium supplemented with 10% FBS and then incubated with the cells for 24 or 48 h.

5.5. Luciferase assay

PC-3 and PC-3-Gluc cells were plated on 96-well culture dishes. For transfection of pCMV-Gluc, each nanoplex of pCMV-Gluc was diluted in 1 mL of medium supplemented with 10% FBS and then incubated with PC-3 cells for 24 h. For transfection of pGL3-basic (Promega, Madison, WI, USA), each nanoplex of pCMV-basic was diluted in 1 mL of medium supplemented with 10% FBS and then incubated with PC-3-Gluc cells for 24 h or 48 h. The level of Gluc activity was evaluated by luciferase activity in the medium, which was measured as counts per sec (cps)/culture medium (mL) using a Gaussia Luciferase Assay Kit (New England BioLabs, Inc., MA, USA). Gluc activity (%) was calculated as relative to the Gluc activity (cps/mL) of NP.

5.6. Immunoblotting

PC-3 cells were seeded in a 35-mm culture dish and incubated overnight. The cells at 30% confluency were transfected with nanoplexes containing pGL3-basic in the presence or absence of the HDAC inhibitor and then incubated for 24 h. The cells were suspended in lysis buffer (1% Triton-X 100 in phosphate-buffered saline pH 7.4 (PBS)), and then centrifuged at 15,000 rpm for 10 min. The supernatants (3 μg protein) were resolved on a 12% sodium dodecyl sulfate–polyacrylamide gel by electrophoresis (SDS–PAGE) and transferred to a polyvinylidene difluoride (PVDF) membrane (FluoroTrans® W, PALL Gelman Laboratory, Ann Arbor, MI, USA). Acetylated histone H3 was detected by rabbit anti-human acetyl histone H3 antibody (Sigma Chemical Co., St. Louis, MO, USA). The goat anti-rabbit IgG peroxidase conjugate (Santa Cruz Biotechnology, Inc., Santa Cruz, CA, USA) was used as secondary antibody. These proteins were detected with peroxidase-induced chemiluminescence (Super Signal West Pico Chemiluminescent Substrate, Pierce, Rockford, IL, USA).

5.7. Cytotoxicity

Cytotoxicity upon transfection using NP-K-182-DD was evaluated with a cell proliferation assay kit (Dojindo, Kumamoto, Japan). PC-3 cells were placed in a 96-well plate in medium containing 10% FBS, and were transfected at various concentrations of nanoplex. After 24 h of incubation, the medium was removed, and the cells were treated with a WST-8 (2-(2-methoxy-4-nitrophenyl)-3-(4-nitrophenyl)-5-(2,4-disulfophenyl)-2*H*-tetrazolium, monosodium salt) solution (10 μL) in medium containing serum (100 μL) for 30 min. Cell viability was expressed as relative to the absorbance at 450 nm of untransfected cells.

5.8. Evaluation of histone deacetylase inhibitory activities

The IC_{50} values were measured by using CycLex HDAC Assay Kit (CycLex Co. Ltd., Nagano, Japan) according to the manufacturer's protocol. The IC_{50} values represent the molar concentrations (μM) required to inhibit the HDACs by 50%.

Acknowledgments

This research was supported by a Grant-in-Aid for Scientific Research (C) 19590110 and "Strategic Project to Support the Formation of Research Bases at Private Universities": Matching Fund Subsidy from MEXT (Ministry of Education, Culture, Sports, Science and Technology), 2008–2012.

References

[1] I.M. Verma, N. Somia, Nature 389 (1997) 239–242.
[2] H. Chong, R.G. Vile, Gene Ther. 3 (1996) 624–629.
[3] E. Otto, A. Jones-Trower, E.F. Vanin, K. Stambaugh, S.N. Mueller, W.F. Anderson, G.J. McGarrity, Human Gene Ther. 5 (1994) 567–575.
[4] E.S. Song, V. Lee, C.D. Suth, A. Lynn, D. Brumm, D.J. Jolly, J.F. Warner, S. Chada, Proc. Natl. Acad. Sci. U.S.A. 94 (1997) 1943–1948.
[5] S. Hasegawa, N. Hirashima, M. Nakanishi, Bioorg. Med. Chem. Lett. 12 (2002) 1299–1302.
[6] M. Nakanishi, Curr. Med. Chem. 10 (2003) 1289–1296.
[7] Y. Hattori, H. Kubo, K. Higashiyama, Y. Maitani, J. Biomed. Nanotechol. 1 (2005) 176–184.
[8] I.S. Zuhorn, R. Kalicharan, D. Hoekstra, J. Biol. Chem. 277 (2002) 18021–18028.
[9] Y. Hattori, A. Hagiwara, W. Ding, Y. Maitani, Bioorg. Med. Chem. Lett. 18 (2008) 5228–5232.
[10] I.S. Zuhorn, J.R.F.N. Engberts, D. Hoekstra, Eur. Biophys. J. 36 (2007) 349–362.
[11] J. Zabner, A.J. Fasbender, T. Moninger, K.A. Poellinger, M.J. Welsh, J. Biol. Chem. 270 (1995) 18997–19007.
[12] E. Dauty, A.S. Verkman, J. Biol. Chem. 280 (2005) 7823–7828.
[13] E.E. Vaughan, R.C. Geiger, A.M. Miller, P.L. Loh-Marley, T. Suzuki, N. Miyata, D.A. Dean, Mol. Ther. 16 (2008) 1841–1847.
[14] M. Goedtfischer, S. Minucci, P. Zhu, O.H. Krämer, A. Schimpf, S. Giavara, J.P. Sleeman, F. Lo-Coco, C. Nervi, P.G. Pelicci, T. Heinzel, EMBO J. 20 (2001) 6969–6978.
[15] A. Saito, T. Yamashita, Y. Mariko, Y. Nosaka, K. Tsuchiya, T. Ando, T. Suzuki, T. Tsuruo, O. Nakanishi, Proc. Natl. Acad. Sci. U.S.A. 96 (1999) 4592–4597.
[16] A. Kalita, C. Ronfis, C. Mastoun, M. Fournel, G. Rahil, T.P. Yan, A. Lu, G.P. Reid, J.M. Besterman, Z. Li, Abstract of AACR-NCI-EORTC Conference, Philadelphia, USA, 2005. C236.
[17] T. Beckers, C. Burkhardt, H. Wieland, P. Gimmnich, T. Ciossek, T. Maier, K. Sanders, Int. J. Cancer 121 (2007) 1138–1148.
[18] M. Yoshida, M. Kijima, M. Akita, T. Beppu, J. Biol. Chem. 265 (1990) 17174–17179.
[19] V.M. Richon, S. Emiliani, E. Verdin, Y. Webb, R. Breslow, R.A. Rifkind, P.A. Marks, Proc. Natl. Acad. Sci. U.S.A. 95 (1998) 3003–3007.
[20] Y. Nagaoka, T. Maeda, Y. Kawai, D. Nakashima, T. Ohkawa, K. Shimoke, T. Ikeuchi, H. Kuwajima, S. Uesato, Eur. J. Med. Chem. 41 (2006) 697–708.
[21] T. Maeda, Y. Nagaoka, Y. Kawai, N. Takagaki, C. Yasuda, S. Yogosawa, Y. Sowa, T. Sakai, S. Uesato, Biol. Pharm. Bull. 28 (2005) 849–853.
[22] T. Maeda, Y. Nagaoka, H. Kuwajima, C. Seno, S. Maruyama, M. Kuronkid, S. Uesato, Bioorg. Med. Chem. 12 (2004) 4351–4360.
[23] W.A. Henne, D.D. Doorneweerd, A.R. Hilgenbrink, S.A. Kularatne, P.S. Low, Bioorg. Med. Chem. Lett. 16 (2006) 5350–5355.
[24] C.P. Leamon, J.A. Reddy, I.R. Vlahov, M. Vetzel, N. Parker, J.S. Nicoson, L.C. Xu, E. Westrick, Bioconjugate Chem. 16 (2005) 803–811.
[25] Y. Hattori, W. Ding, Y. Maitani, J. Controlled Release 120 (2007) 122–130.
[26] C.A. Hassig, S.L. Schreiber, Curr. Opin. Chem. Biol. 1 (1997) 300–308.
[27] T. Kouzarides, Curr. Opin. Genet. Dev. 9 (1999) 40–48.
[28] R.D. Strahl, C.D. Allis, Nature (London) 403 (2000) 41–45.
[29] L.R. Jones, E.A. Goun, R. Shinde, J.R. Rothbard, C.H. Contag, H. Christopher, P.A. Wender, J. Am. Chem. Soc. 128 (2006) 6526–6527.

Journal of Controlled Release 136 (2009) 30–37

Contents lists available at ScienceDirect

Journal of Controlled Release

journal homepage: www.elsevier.com/locate/jconrel

Novel irinotecan-loaded liposome using phytic acid with high therapeutic efficacy for colon tumors

Yoshiyuki Hattori *, Li Shi, Wuxiao Ding, Kimiko Koga, Kumi Kawano, Motoki Hakoshima, Yoshie Maitani

Department of Fine Drug Targeting Research, Institute of Medicinal Chemistry, Hoshi University, Ebara 2-4-41, Shinagawa-ku, Tokyo, 142-8501, Japan

ARTICLE INFO

Article history:
Received 7 October 2008
Accepted 18 January 2009
Available online 24 January 2009

Keywords:
Liposomes
Phytic acid
CPT-11
Irinotecan
Colon tumor

ABSTRACT

Phytic acid (IP-6) is a polyphosphorylated carbohydrate with antitumor activity for many kinds of tumors. In this study, we developed a novel method of loading irinotecan (CPT-11) into liposomes using IP-6, and evaluated its antitumor effect on colon tumors in vivo. Liposomal CPT-11 was prepared by loading CPT-11 to distearoylphosphatidylcholine/cholesterol/methoxy-poly(ethyleneglycol)-distearylphosphatidylethanolamine liposomes prepared in IP-6 solution, $CuSO_4$ solution and citrate buffer, respectively (IP6-, Cu- and Cit-L). CPT-11 loading efficiency for IP6-L (90–100%) was higher than that for Cit-L (less than 40%), and similar to Cu-L when CPT-11 to total lipid weight ratio was increased from 0.2 to 0.6. Plasma elimination and biodistribution of liposomal CPT-11 and its metabolite SN-38 were measured after intravenous administration. IP6-L following i.v. injection showed 1.3- and 1.7-fold higher plasma area under the curves of CPT-11 and SN-38, respectively, than Cu-L. Finally, therapeutic activity was determined in mouse Colon 26 and human COLO 320DM tumor xenografts in mice. IP6-L significantly exhibited superior anticancer activity to Cu-L and free CPT-11 in Colon 26 tumor. Using IP-6 as a drug-trapping agent in liposome, IP6-L improved CPT-11 pharmacokinetics and increased antitumor activity in colon tumors.

1. Introduction

Irinotecan (CPT-11) is a water-soluble derivative of camptothecin, which is a natural alkaloid originally extracted from the Chinese tree *Camptotheca acuminata*. CPT-11 inhibits the resealing of single-strand DNA breaks mediated by topoisomerase I by stabilizing cleavable complexes [1–3]. CPT-11 has excellent antitumor activity against a variety of human xenografts via intravenous, intraperitoneal and oral administration. The clinical introduction of CPT-11 had a significant impact on cancer treatment, particularly colorectal adenocarcinoma [4,5]. CPT-11 is subjected to an enzymatic conversion that yields a number of metabolites, including SN-38 [6,7], which is reported to be up to 1000-fold more active than CPT-11 *in vitro* [8]. Therefore, CPT-11 requires conversion to SN-38 for optimal activity yet must avoid inactivation via simple hydrolysis of the requisite lactone configuration to an inactive carboxylate. After intravenous administration of free CPT-11, less than 5% of CPT-11 is converted to SN-38, mainly in the liver. PEGylated liposomal CPT-11 has long circulation in the blood and will therefore improve conversion from CPT-11 to SN-38, and increase antitumor activity. Use of drug delivery technologies, such as a PEGylated carrier system including liposome, have focused on strategies to stabilize the lactone ring of CTP-11.

It has already been established that CPT-11 was encapsulated within liposomes using a remote loading method. CPT-11 can be actively loaded into liposomes via a transmembrane pH gradient using citrate [9], ammonium sulfate or ionophore A23187/divalent cation [10–12]. The acidified liposomal interior causes the loading and retention of CPT-11 with ionizable amine groups, however, the acidified liposome can introduce instability by hydrolyzing lipid at acidic pH during long-term storage. Recently, a loading method was developed using copper adjusted to neutral pH with triethanolamine (TEA) without generation of a pH gradient [10,13]; however, there is a possibility that serum copper causes systemic toxicity [14–16]. As an alternative, CPT-11 loading systems have been successful using a polyanionic trapping agent of either polyphosphate or sucrose octasulfate, adjusted to neutral pH with triethylammonium [17].

Phytic acid (inositol hexakisphosphate, IP-6) is also a naturally occurring negatively charged polyphosphorylated carbohydrate, and has been reported to reduce abnormal gene expression and to induce the expression of tumor suppressive gene in tumors [18–20]. In combination with doxorubicin in breast tumor cells, IP-6 synergically inhibited tumor growth [21,22]. We expected that negatively charged IP-6 could electrostatically interact with CPT-11 as a intraliposomal drug-trapping agent like polyphosphate [17] and might increase antitumor activities if it is co-encapsulated with CPT-11 in liposomes. In this report, therefore, we developed a novel CPT-11 loading system using IP-6 as a polyanionic trapping agent, and adjusted to pH 6.5 with TEA. A novel liposomal CPT-11 with IP-6 (IP6-L) was evaluated in terms of plasma elimination and the biodistribution of CPT-11 and its metabolite SN-38 after intravenous administration. Furthermore, the therapeutic activity of IP6-L was evaluated in mouse Colon 26 tumor and human COLO 320DM tumor xenografts in mice.

* Corresponding author. Tel./fax: +81 3 5498 5097.
E-mail address: yhattori@hoshi.ac.jp (Y. Hattori).

0168-3659/$ – see front matter © 2009 Elsevier B.V. All rights reserved.
doi:10.1016/j.jconrel.2009.01.013